Exploring the iron intercellular communication in the liver

Leonor Teixeira da Silva e Almeida Gomes
Master in Biochemistry
Faculty of Sciences of University of Porto and School of Medicine and Biomedical Sciences
2024/2025

Exploring the iron intercellular communication in the liver

Leonor Teixeira da Silva e Almeida Gomes

Dissertation carried out as part of the MSc in Biochemistry

Department of Chemistry and Biochemistry Faculty of Sciences of University of Porto and School of Medicine and Biomedical Sciences – University of Porto

2024/2025

Supervisor
Ana Carolina Moreira, PhD
Junior Researcher at i3S – Instituto de Investigação e Inovação em Saúde, Porto, Portugal;
Invited Assistant Professor at ICBAS – Instituto de Ciências Biomédicas Abel Salazar, University of Porto

Co-supervisor
Maria Salomé Gomes, PhD
Leader of the Host Targets of Infection Group, i3S – Instituto de Investigação e Inovação em Saúde, Porto Portugal;
Full Professor at ICBAS – Instituto de Ciências Biomédicas Abel Salazar, University of Porto

External Host Supervisor
Martina Muckenthaler, PhD
Professor of Molecular Medicine, University Medical Center Heidelberg
Principal Investigator and Head of Molecular Medicine Partnership Unit (MMPU), Germany
Group Leader, Germany

INSTITUTO DE INVESTIGAÇÃO E INOVAÇÃO EM SAÚDE
UNIVERSIDADE DO PORTO

UNIVERSITÄT HEIDELBERG
ZUKUNFT SEIT 1386

Funding

This project was conducted at i3S - Institute for Research and Innovation in Health, and University of Heidelberg (Heidelberg, Germany).

This work was funded through National funds by Fundação para a Ciência e Tecnologia through the project “IronCell2Cell: The macrophage-hepatocyte iron communication during mycobacterial infection”, identified with the following DOI: 2022.03635.PTDC.

Part of this project was carried out during an ERASMUS-funded student mobility at University of Heidelberg (Heidelberg, Germany), between January and June 2025.

Scientific Outreach

Part of the introduction of this thesis is published in a review article:

Fonseca, Ó.; Ramos, A.S.; Gomes, L.T.S.; Gomes, M.S.; Moreira, A.C. New Perspectives on Circulating Ferritin: Its Role in Health and Disease. Molecules 2023, 28, 7707.

Acknowledgements

Agradeço à Faculdade de Ciências da Universidade do Porto, ao Instituto de Ciências Biomédicas Abel Salazar, bem como à Universidade do Porto como um todo por me terem acolhido durante os últimos cinco anos e por me terem proporcionado as ferramentas necessárias para a minha formação.

Agradeço de igual forma ao i3S e à Universidade de Heidelberg por me terem recebido para que pudesse realizar a minha dissertação de mestrado.

Gostaria ainda de deixar um reconhecimento a todas as pessoas que fizeram parte deste percurso.

Muito obrigada, professora Salomé, pela oportunidade de continuar a integrar o seu grupo de investigação, pelo acompanhamento próximo, pela disponibilidade constante e pela valiosa orientação.

Carolina, muito obrigada por teres aceitado continuar a ser a minha orientadora, por todas as oportunidades que me proporcionaste e pela tua enorme dedicação em tornar realidade o meu objetivo de fazer Erasmus. Agradeço também a tua confiança nas minhas capacidades e o teu apoio permanente que tanto significam para mim.

I would like to thank Dr. Martina for welcoming me into her research group, for allowing me to experience a new working environment, and for the insightful contributions that enriched my project.

Devo também um especial agradecimento ao Óscar. Sem ti, este percurso teria sido muito mais difícil. Obrigada por tudo o que me ensinaste, por todas as experiências nas quais me acompanhaste e por atenderes a todos os meus pedidos.

Thank you very much, Qiu and Stefania, for everything you taught me in the lab, for your support, guidance, and insight. I truly appreciate the contributions you have made to this project.

Obrigada, Isabel, por me acompanhares neste percurso, tanto nalgumas experiências, como nos lanches, na aventura de Erasmus e no curso de estatística. Obrigada, também pela ajuda nas emergências informáticas, que é sempre muito valiosa.

Gostaria também de agradecer à Tânia, à Clara e ao Gabriel por estarem sempre disponíveis para me ajudar e pelo vosso contributo neste projeto.

Obrigada, Mariana, também por me acompanhares nestes dois anos, nas aulas, no laboratório, na aventura de Erasmus e nos lanches.

Obrigada a todos os HOTI por serem, cada um à sua maneira, um exemplo para mim, por todos os conselhos que me deram e pela boa disposição constante, tornando os dias no laboratório tremendamente mais agradáveis.

To all the members of the Iron Metabolism group in Heidelberg, thank you for welcoming me and for all the help and support throughout my Erasmus.

Obrigada ao Pedro, à Camila, à Cecília, à Cristina, à Isabel, ao Gui, à Mariana, ao Miguel, à Rosa e ao Tito por terem partilhado este percurso comigo, pelas conversas, reclamações, gargalhadas e por todos os momentos que tornaram estes dois anos mais incríveis.

Finalmente, um agradecimento à minha família pelo apoio incondicional ao longo destes últimos anos.

Resumo

A homeostasia de ferro é crucial para o bom funcionamento dos organismos, sendo que o fígado é o órgão central na manutenção desta homeostasia, regulando os níveis de ferro sistémico. Está bem documentado que durante períodos de infeção e inflamação, a homeostasia de ferro é perturbada. Contudo, o modo como diferentes células comunicam para induzir essas mudanças permanece pouco estudado. Assim, o objetivo deste projeto era explorar a comunicação relacionada com o ferro no fígado, em particular, durante infeção ou inflamação. Decidimos focar-nos em macrófagos, hepatócitos e células endoteliais do sinusoide do fígado (LSEC), uma vez que estas células desempenham funções relevantes no metabolismo de ferro, infeção e inflamação.

Deste modo, o primeiro passo deste trabalho consistiu em estabelecer e otimizar culturas primárias dos três tipos celulares em estudo. De seguida, avaliámos a expressão de genes do metabolismo de ferro (genes *Fth*, *Ftl*, *Bmp6*, *Fpn* e *Tfr1*) por qRT-PCR e avaliámos a síntese e libertação de ferritina-H e -L (FTH e FTL) por ELISA e western blot nos lisados e sobrenadantes das células. As células foram analisadas em condições basais e após estimulação com excesso de ferro, LPS, TNF-α, FSL-1 ou infeção por *M. avium*. Por último, investigámos a comunicação intercelular entre hepatócitos e macrófagos durante infeção, bem como entre hepatócitos e LSEC aquando de inflamação.

Em condições basais, hepatócitos e macrófagos apresentaram perfis de expressão genética semelhantes, com níveis mais elevados de *Fth1* e *Ftl*, comparados com os níveis de *Bmp6*, *Fpn* e *Tfr1*. A proteína ferritina (FT) foi também detetada em lisados de hepatócitos e macrófagos. É relevante mencionar que esta proteína foi ainda detetada em sobrenadantes de culturas dos três tipos celulares, indicando que estes são capazes de libertar ambas as subunidades de FT.

Em macrófagos, não foram observadas diferenças significativas na expressão de genes relacionados com ferro após infeção por *M. avium.* Em hepatócitos, sobrecarga de ferro levou a um aumento na expressão de *Fth1* e *Ftl* e a uma diminuição na expressão de *Tfr1.* Observou-se também um aumento da concentração intracelular de FTL. A estimulação de hepatócitos com LPS conduziu a um aumento de expressão de *Tfr1*, sem nenhuma outra alteração nos genes relacionados com ferro. Em LSEC, excesso de ferro juntamente com meio condicionado de hepatócitos levou a uma sobre regulação

da expressão de *Bmp6*. Além disso, estimulação de LSEC com TNF-α e FSL-1 aumentou a libertação de FTH e FTL, respetivamente.

Relativamente à comunicação intercelular, observámos que hepatócitos cultivados com meio condicionado de LSEC tratados com TNF-α e FSL-1 tendiam a expressar menos *Fth1* e *Fpn*, comparados com hepatócitos cultivados com meio de LSEC não estimuladas.

A co-cultura de hepatócitos com macrófagos infetados por *M. avium* não levou a alterações significativas na expressão de genes relacionados com o metabolismo de ferro.

Em conclusão, apesar de este ser um estudo exploratório e de alguns aspetos necessitarem de otimizações e repetições, este trabalho mostra que inflamação e infeção conduzem a mudanças no metabolismo de ferro e que a comunicação entre células tem um papel importante nessas mudanças.

Palavras-chave: Ferro, infeção, inflamação, fígado, comunicação intercelular.

Abstract

Iron homeostasis is crucial for organisms' proper functioning, with the liver acting as the central regulator of systemic iron levels. It is well documented that during infection and inflammation, iron metabolism is disrupted. However, how different cell types communicate to induce those changes remains poorly understood. Thus, the general aim of this project was to explore the iron-related intercellular communication in the liver, particularly upon infection and inflammation. We decided to focus on macrophages, hepatocytes, and liver sinusoidal endothelial cells (LSEC) as these play important roles in iron metabolism, infection, and inflammation.

Therefore, firstly, we established and optimized primary cell cultures of the three cell types. We then evaluated the expression of the iron-related genes *Fth*, *Ftl*, *Bmp6*, *Fpn* and *Tfr1*, by qRT-PCR, and evaluated H- and L-ferritin (FTH and FTL) synthesis and release through ELISA and western blot, in cell lysates and supernatants. Cells were analyzed under basal conditions and after stimulation with iron overload, LPS, TNF-α, FSL-1, or infection with *M. avium*. Finally, we studied intercellular communication between hepatocytes and macrophages and between hepatocytes and LSEC.

Under basal conditions, hepatocytes and macrophages showed similar iron-related gene expression profiles, with higher levels of *Fth1* and *Ftl*, as compared to the levels of *Bmp6*, *Fpn* and *Tfr1*. Ferritin (FT) protein was also detected in macrophage and hepatocyte lysates. Importantly, this protein was also detected in the supernatants of the cultures of all three cell types, indicating that they are capable of releasing both FT subunits.

In macrophages, no significant alterations were observed in iron-related gene expression, upon infection with *M. avium.* In hepatocytes, iron overload led to an increase in the expression of *Fth1* and *Ftl* and a decrease in the expression of *Tfr1*. An increase in the intracellular concentration of FTL was also observed. The stimulation of hepatocytes with LPS led to an increase in the gene expression of *Tfr1*, with no additional alterations in iron-related genes. In LSEC, iron overload, together with hepatocyte conditioned medium, led to an upregulation of *Bmp6* gene expression. Moreover, stimulation of LSEC with TNF-α and FSL-1 increased the release of FTH and FTL, respectively.

Concerning intercellular communication, we observed that hepatocytes cultured in the presence of conditioned medium from TNF-α- or FSL-1-treated LSEC tended to

downregulate *Fth1* and *Fpn,* as compared to hepatocytes cultured with conditioned medium from non-stimulated LSEC.

The co-culture of hepatocytes with *M. avium*-infected macrophages did not lead to any significant change in iron-related gene expression.

In conclusion, although this was an exploratory study and some aspects require further optimization and repetition, this work shows that inflammation and infection lead to changes in iron metabolism and that intercellular communication plays a role in those changes.

Keywords: Iron, infection, inflammation, liver, intercellular communication.

Table of Contents

List of Tables xi

List of Figures xii

List of Abbreviations xiv

Introduction 1

1. Iron metabolism 2

1.1 Regulation of iron homeostasis 4

2. The liver 8

2.1 Liver structure and cell types 8

2.2 Intercellular communication in the liver 10

3. Iron metabolism during inflammation 12

4. Iron metabolism deregulation during infection 13

4.1 Iron metabolism during infection 13

4.2 Iron redistribution during Mycobacterial infection 14

5. Cell cultures 15

6. Thesis aims and structure 18

Materials and Methods 19

Reagents 20

Primary mouse cells 20

Bone marrow-derived macrophages (BMM) 20

BMM infection 21

BMM lysate and supernatant collection 21

Plate collagen-coating 21

Liver harvesting 22

Primary hepatocyte (PH) culture 23

PH and BMM co-culture 24

Collection of PH lysates and conditioned media 24

LSEC culture 25

LSEC treatment 26
Conditioned media and iron 26
TNF-α and Fibroblast-Stimulating Lipopeptide-1(FSL-1) 26
LSEC collection 26
LSEC's conditioned media collection 27
PH treatment with LSEC conditioned media and cell collection 27
Viability assay 27
Fluorescence-activated Cell Sorting (FACS) 28
Supernatant concentration 29
Protein quantification 29
Western blot 30
Enzyme-linked immunosorbent assay (ELISA) 31
RNA extraction 32
cDNA synthesis 32
Quantitative Real Time (qRT) -PCR 33
Intracellular iron quantification 35
Statistical analysis 35
Results 36
1. Optimization of primary cell cultures 37
1.1 BMM culture 37
1.2 Primary hepatocyte culture 37
2. Iron-related characterization under basal conditions 41
2.1 Iron-related gene expression 41
2.2 FT synthesis and release 43
2.3 Intracellular iron quantification 44
3. Iron-related characterization upon various stimuli 45
3.1 Iron-related gene expression 45
3.2 FT synthesis and release 47
3.2 Intracellular iron quantification 51

4. Iron-related gene expression in hepatocytes upon intercellular communication... 52

Discussion 55

Conclusion and Future Perspectives..... 68

References 70

List of Tables

Table 1 - List of primers' sequences used with BMM and PH samples. 34
Table 2 - List of primers' sequences used with LSEC samples. 34
Table 3 - FTs quantification on lysates and supernatants of BMM, hepatocytes, and LSEC under basal conditions. 43
Table 4 - Intracellular iron content in BMM, hepatocytes (PH), and LSEC under basal conditions. 44

List of Figures

Figure 1 - Iron metabolism. 4

Figure 2 - Hepcidin induction in hepatocytes by BMP2/6. 6

Figure 3 - The liver. 8

Figure 4 - Iron metabolism and intercellular communication in the liver. 11

Figure 5 - Macrophage to hepatocyte communication. 12

Figure 6 - Timeline for bone marrow-derived macrophages culture maintenance. 37

Figure 7 - Primary hepatocyte culture. Light microscope image, with a 400x magnification, of the primary hepatocyte culture, the day after isolation. 38

Figure 8 - Ferric Ammonium Citrate (FAC) does not alter hepatocyte viability. 38

Figure 9 - Primary liver sinusoidal endothelial cell (LSEC) culture. 39

Figure 10 - Fluorescence-Activated Cell Sorting (FACS) analysis of primary liver sinusoidal endothelial cells (LSECs) 1 day post-isolation. 41

Figure 11 - qRT-PCR analysis of iron-related genes expression in BMM under basal conditions. 41

Figure 12 - qRT-PCR analysis of iron-related genes expression in hepatocytes under basal conditions. 42

Figure 13 - qRT-PCR analysis of *Bmp6* expression in LSEC under basal conditions. 42

Figure 14 - Western blot of FTH, FTL and CD63 on BMM and hepatocytes supernatants. 44

Figure 15 - qRT-PCR analysis of iron-related gene expression in infected BMM. 45

Figure 16 - qRT-PCR analysis of iron-related gene expression in hepatocytes following iron overload (FAC) or LPS treatment (LPS). 46

Figure 17 - qRT-PCR analysis of iron-related genes expression in LSEC. 46

Figure 18 - FT quantification in BMM. 49

Figure 19 - FT quantification in hepatocytes. 50

Figure 20 - FT quantification on LSEC supernatant upon inflammatory stimuli..... 51

Figure 21 - Iron intracellular quantification in stimulated BMM. 52

Figure 22 - Iron intracellular quantification in stimulated LSEC. 52

Figure 23 - qRT-PCR analysis of iron-related gene expression in hepatocytes following co-culture or conditioned media treatment. 54

List of Abbreviations

APC	ALLOPHYCOCYANIN
APP	ACUTE PHASE PROTEINS
BMM	BONE MARROW-DERIVED MACROPHAGE
BMP	BONE MORPHOGENETIC PROTEIN
BSA	BOVINE SERUM ALBUMIN
CT	CYCLE TRESHHOLD
DCYTB	DUODENAL CYTOCHROME B
DGAV	DIREÇÃO-GERAL DE ALIMENTAÇÃO E VETERINÁRIA
DMEM	DULBECCO'S MODIFIED EAGLE MEDIUM
DMT-1	DIVALENT METAL TRANSPORTER 1
DNTP	DEOXYNUCLEOSIDE TRIPHOSPHATES
EC	ENDOTHELIAL CELL
EDTA	ETHYLENEDIAMINETETRAACETIC ACID
ELISA	ENZYME-LINKED IMMUNOSORBENT ASSAY
EV	EXTRACELLULAR VESICLE
FAC	FERRIC AMMONIUM CITRATE
FACS	FLUORESCENCE-ACTIVATED CELL SORTING
FBS	FETAL BOVINE SERUM
FCUP	FACULTY OF SCIENCES OF THE UNIVERSITY OF PORTO
FELASA	FEDERATION FOR LABORATORY ANIMAL SCIENCE ASSOCIATIONS
FENTA	FERRIC NITRILOTRIACETIC ACID
FITC	FLUORESCEIN
FSL-1	FIBROBLAST-STIMULATING LIPOPEPTIDE
FSC	FRONT SCATTER
FT	FERRITIN
FTH	H-FERRITIN
FTL	L-FERRITIN
FPN	FERROPORTIN
HBSS	HANK´S BALANCED SALT SOLUTION
HIF	HYPOXIA-INDUCIBLE FACTOR
HO-1	HEME OXYGENASE 1
HSC	HEPATIC STELLATE CELL
IL	INTERLEUKIN

IRE	IRON RESPONSIVE ELEMENT
IRP	IRON REGULATORY PROTEIN
INF	INFECTED
KC	KUPFFER CELL
L-CM	LSEC CONDITIONED MEDIA
LCCM	L929 CELL CONDITIONED MEDIUM
LPS	LIPOPOLYSACCHARIDE
LSEC	LIVER SINUSOIDAL ENDOTHELIAL CELL
MCSF	MACROPHAGE COLONY STIMULATING FACTOR
MW	MOLECULAR WEIGHT
NCOA4	CARGO NUCLEAR RECEPTOR COACTIVATOR 4
NI	NON-INFECTED
NRAMP	NATURAL RESISTANCE-ASSOCIATED MACROPHAGE PROTEIN
NT	NON-TREATED
NTM	NON-TUBERCULOUS MYCOBACTERIA
PAMP	PATHOGEN-ASSOCIATED MOLECULAR PATTERN
PBS	PHOSPHATE BUFFERED SALINE
PE	PHYCOERYTHRIN
PH	PRIMARY HEPATOCYTE
PIC	PROTEASE INHIBITOR COCKTAIL
PRR	PATTERN RECOGNITION RECEPTOR
QRT	QUANTITATIVE REAL-TIME
ROS	REACTIVE SPECIES OF OXYGEN
R-SMAD	RECEPTOR-ASSOCIATED SMAD PROTEIN
RT	ROOM TEMPERATURE
SSC	SIDE SCATTER
TBS-T	TRIS BUFFERED SALINE WITH TWEEN 20
TF	TRASFERRIN
TFR	TRANSFERRIN RECEPTOR
TGF	TUMOR GROWTH FACTOR
TLR	TOLL-LIKE RECEPTOR
TNF	TUMOR NECROSIS FACTOR
UP	UNIVERSITY OF PORTO
UTR	UNTRANSLATED REGION
VEGF	VASCULAR ENDOTHELIAL GROWTH FACTOR

Introduction

1. Iron metabolism

Iron is required for the synthesis of hemoproteins, iron-sulfur clusters, and other iron-dependent proteins, which are indispensable for vital processes including mitochondrial respiration and DNA synthesis. In fact, the lack of this element may result in cellular growth arrest and even cell death, highlighting its importance. Iron's participation in a variety of processes is due to its properties as a transition metal. This characteristic allows it to easily take part in redox reactions, oscillating between the ferrous (Fe^{2+}) and ferric (Fe^{3+}) states. Iron´s lability, although very advantageous, can also lead to harmful consequences for the organisms. For example, during the Fenton reaction, iron reacts with hydrogen peroxide, producing reactive oxygen species (ROS). Thus, both deficiency and excess of this element are harmful, and it is of extreme importance that its metabolism network is delicately regulated (Figure 1) [2, 3].

In mammals, dietary iron is absorbed by enterocytes, which take up non-heme iron, usually in the ferric state, heme iron, and iron bound to proteins. The absorption of non-heme iron starts with its reduction to ferrous iron by the duodenal cytochrome b (DCYTB), followed by its internalization performed by the divalent metal transporter 1 (DMT-1) [3]. Regarding the heme group absorption, the actual internalization mechanism is not well known, but once inside the enterocytes, it is degraded by heme oxygenase 1 (HO-1), releasing iron [4]. Once iron is inside the enterocytes, it may be exported to the bloodstream by ferroportin (FPN), the only known iron exporter [3].

Mammals do not only rely on iron´s intestinal absorption for all the element´s requirements. The recycling of damaged or senescent erythrocytes, erythrophagocytosis, contributes greatly to the organism’s iron pool, and it is performed by specialized macrophages. After phagocytosis, hemoglobin is degraded, and the heme-bound iron is either stored or secreted by FPN to enter the bloodstream [4].

In the bloodstream, iron is mainly transported bound to transferrin (Tf). Tf-bound iron is in a soluble form, less reactive, and difficult to extract, so it will not be prone to engage in harmful reactions. When necessary, Tf binds to its ubiquitous receptor in cells, the transferrin receptor 1 (TfR1), and the complex is internalized by endocytosis. Inside the endosome, the lower pH induces a conformational change in Tf and allows iron release. Following the internalization, DMT-1 transports iron across the endosomal membrane into the cytoplasm, and apo-Tf and TfR1 are recycled back to the membrane to participate in a new transport and uptake cycle [5]. Of note, there is another transferrin

receptor, the transferrin receptor 2 (TfR2), which is thought to have more of a regulatory function, being important for iron sensing in hepatocytes [6].

Once iron is inside the cells, it may be used in different processes, including erythropoiesis in the bone marrow [4]. Iron in excess is stored. The storage occurs primarily in hepatocytes and resident macrophages. Hepatocytes serve as the main reservoir for iron, and the metal is mobilized according to the organism's needs [7, 8]. Within cells, iron is stored inside ferritin (FT). FT is a central protein in iron metabolism as it prevents the element from being free in the cell [9]. Importantly, even though FT is primarily an intracellular protein, it is found in the serum [10], where it may indicate inflammation and potentially play regulatory roles [1]. The mechanism through which FT is released into circulation remains a debate. Some authors declare that the storage protein is passively released after cell death [11], while others argue FT is purposefully released. Although FT´s secretion process is not clear, some authors have shown that the protein can be carried out of the cells inside extracellular vesicles (EVs) [12-14]. Of note, EVs are nanoparticles that cells secrete, with a role in intercellular communication [15].

In structural terms, the storage protein is a 24-meric sphere-like heteropolymer that can lodge up to around 3000 iron atoms [16]. The polymer is composed of two types of subunits, the L-ferritin (FTL) and the H-ferritin (FTH) [17]. The ratio between FTL (19 kDa) and FTH (21 kDa) chains in the polymer may vary according to cell type, physiological state, and response to infection/inflammation [3]. Notably, the two ferritin subunits have different functions. FTH has a ferroxidase activity, oxidizing Fe^{2+} before its internalization, whereas FTL does not have enzymatic activity and plays a more structural role [18]. Whenever the cells' iron requirements increase, iron must be released from the storage protein. Here, FT is transported into autophagosomes by cargo nuclear receptor coactivator 4 (NCOA4) and undergoes a process named ferritinophagy, releasing the iron [19].

Iron secretion, in mammals, lacks a specific mechanism. However, the metal can be lost due to bleeding, sweat, and cell desquamation [20]. Iron's intestinal absorption accounts for these losses and its levels in the organism remain relatively constant in healthy conditions [3].

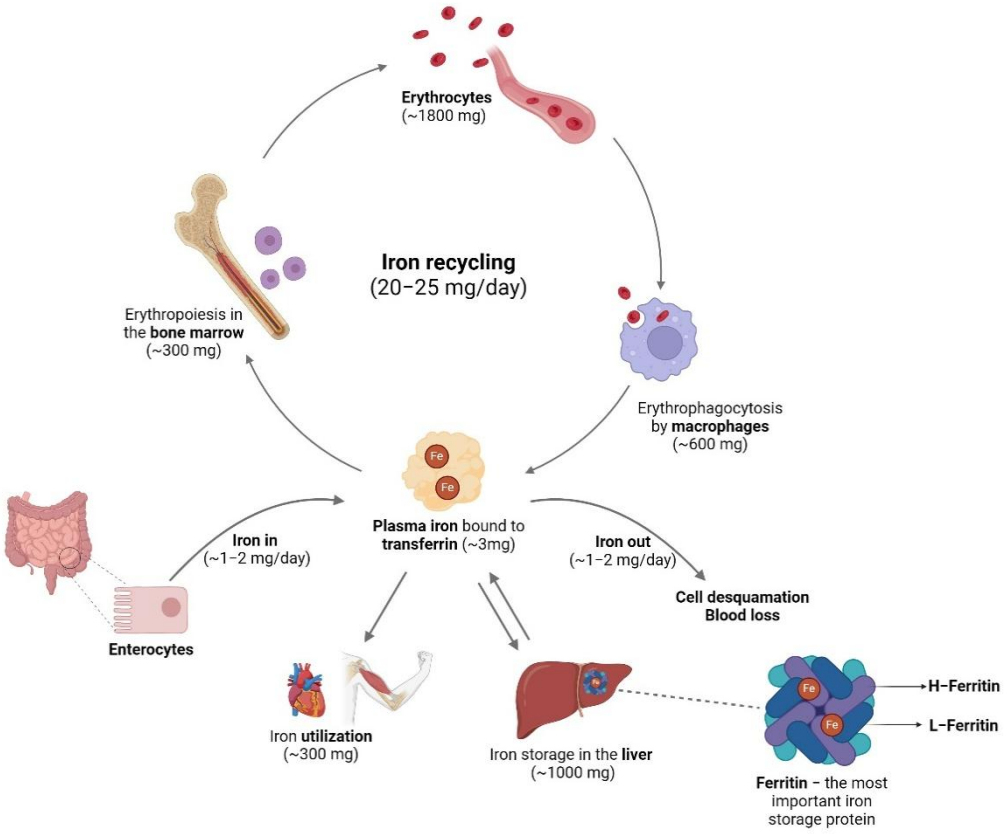


Figure 1 - Iron metabolism. Dietary iron is absorbed by the enterocytes in the small intestine. In the bloodstream, iron is bound to transferrin, which transports the metal to other cells. Iron is mainly stored in the liver, specifically inside the storage protein, ferritin, in hepatocytes. Ferritin is composed by two subunits, the L- and H-ferritin. The metal is used for many processes, but most of the iron pool is used for erythropoiesis in the bone marrow. Macrophages can phagocyte damaged or senescent erythrocytes, recycling the iron they contain. Small losses of the element might occur, namely through cell desquamation and blood losses. From Fonseca, Ramos, Gomes et al, 2023 [1].

1.1 Regulation of iron homeostasis

As discussed above, iron homeostasis is crucial for the proper functioning of an organism, therefore, it must be tightly regulated.

On a systemic level, the main regulator is the hormone hepcidin. Hepcidin is mainly produced by hepatocytes, and when secreted, it binds to FPN on the surface of enterocytes, hepatocytes, and macrophages. This binding leads to FPN´s internalization and degradation. FPN degradation causes a significant reduction in iron export, and the metal accumulates inside the cells. Besides that, the expression of DMT-1 in the apical side of enterocytes is downregulated by hepcidin, resulting in a decreased intestinal absorption of iron [21]. Hence, hepcidin secretion culminates in a reduction in circulating iron levels. By opposition, if hepcidin production is diminished, ferroportin would be more expressed in the cells' membranes, favouring intracellular iron export, and DMT-1 would be more present in the enterocytes, increasing intestinal iron absorption. Thus, systemic iron levels would increase [21, 22].

Hepcidin synthesis and release are regulated by iron availability, inflammatory and infectious stimuli, erythropoietic demand, and hypoxia, among others [22].

Regarding hepcidin´s transcriptional regulation in response to iron availability, the bone morphogenetic protein (BMP) signalling pathway is one of the most important (Figure 2). Upon elevated iron levels in the liver, BMP6 and BMP2 are produced mainly by LSEC. These are the main ligands of this pathway, and they belong to the superfamily of tumor growth factor β (TGF-β). Of note, the lack of either BMP2 or BMP6 is enough to impair the regulation of iron levels, so it is hypothesized that they act as heterodimers. Interestingly, BMP2 is more expressed than BMP6, even when iron levels are increased. However, BMP6 mRNA levels correlate highly with iron levels, so it is thought that BMP6 production is the limiting step in the pathway [23]. BMPs bind to the complex of two type I and two type II receptors in the hepatocyte, as well as to the co-receptor hemojuvelin. Of note, this co-receptor also regulates hepcidin expression, and, when mutated, can impair iron homeostasis [24]. The binding induces type II receptors to phosphorylate the type I receptors, which triggers the phosphorylation of the intracellular signalling molecules, receptor-associated SMAD proteins (R-SMAD). The phosphorylated SMAD 1/5/8 (R-SMADs) and SMAD4 are translocated to the cell nucleus, where they induce hepcidin gene transcription [23].

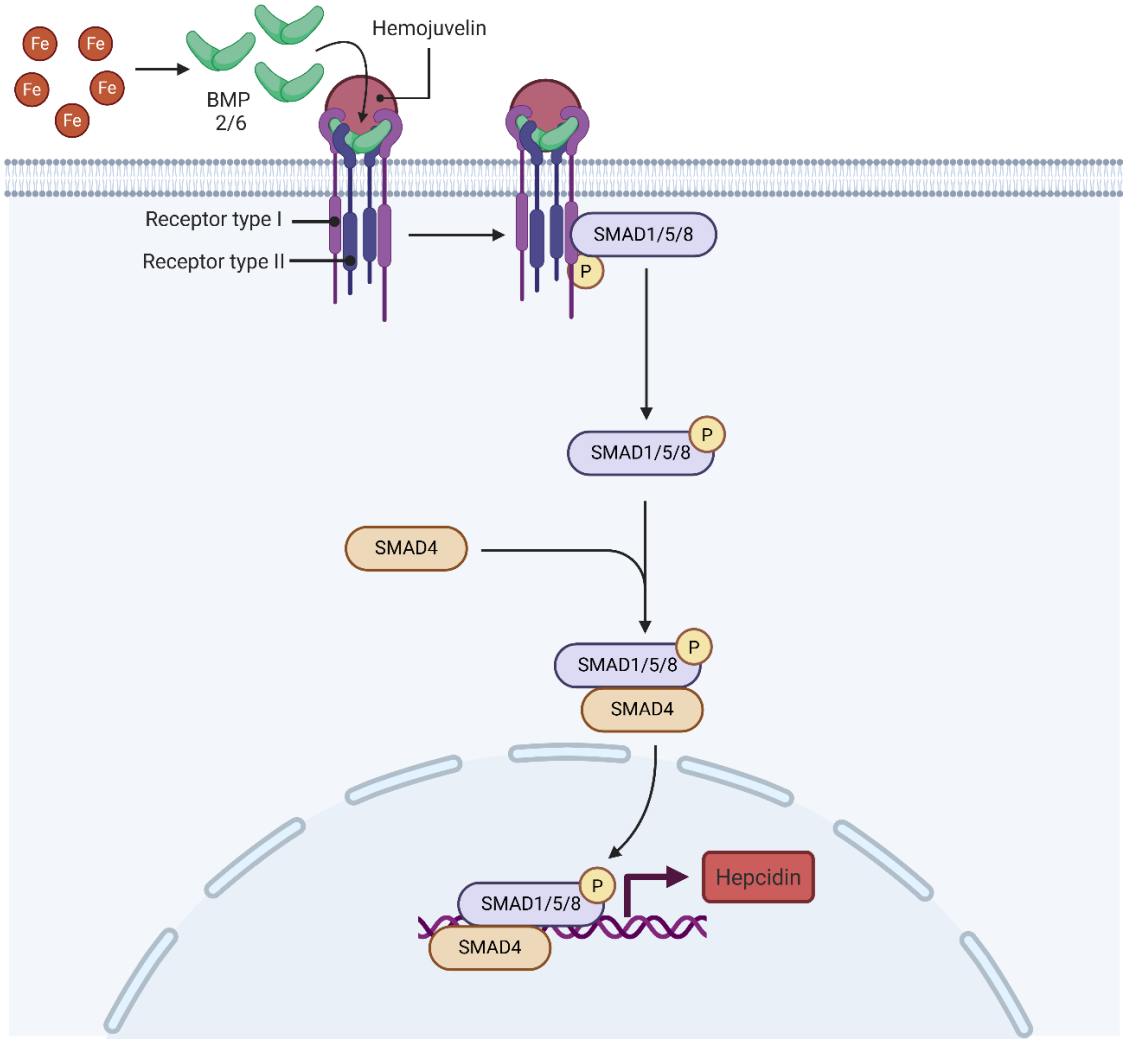


Figure 2 - Hepcidin induction in hepatocytes by BMP2/6. Upon elevated iron levels, BMP2 and BMP6 are produced by LSEC. These ligands bind to their receptors I and II and co-receptor hemojuvelin. Upon binding, the type I receptors phosphorylates the type II receptors, which will then phosphorylate SMAD1/5/8. SMAD1/5/8, together with SMAD4, are translocated to the nucleus, where they bind to the hepcidin's promoter, inducing the expression of the hepcidin's gene. Created with BioRender.com.

Inflammatory cytokines also influence hepcidin levels. For instance, interleukin (IL)-6 promotes the expression of hepcidin by triggering STAT3 phosphorylation, which is followed by the protein's translocation to the nucleus, where it can bind to the STAT3-binding motif in the hepcidin promoter, activating the gene transcription [25, 26].

The production of inflammatory cytokines can be triggered by infection, namely by the activation of Toll-like receptor (TLR) 4 by lipopolysaccharide (LPS), a component of the cell wall of Gram-negative bacteria [27]. *In vivo* studies have demonstrated that hepcidin levels increase upon infection by several pathogens, such as *Salmonella* Typhimurium [28], *Pseudomonas aeruginosa*, group A *Streptococcus* [29], *Klebsiella pneumonia [30]*, *Candida albicans,* or Influenza A virus [31].

Erythropoiesis is a process that requires high quantities of iron. Consequently, whenever the erythropoietic demand is increased, a great amount of iron is needed [32]. Thus, it is essential to increase iron in circulation to accommodate this demand. In this context, the production of hepcidin is decreased, mainly in response to the erythroid factor erythroferrone [33]. It has been proposed that erythroferrone leads to the decrease of hepcidin production by binding and sequestering BMP ligands, thus preventing the BMP pathway activation in the hepatocytes [34]. Moreover, in hypoxic conditions, the production of red blood cells is promoted. Thus, during hypoxia, hepcidin expression is also inhibited by increased production of erythropoietic factors, namely erythropoietin and erythroferrone [35].

At a cellular level, the IRE-IRP system is the most relevant form of iron metabolism regulation. IREs (iron responsive elements) are conserved hairpins in the untranslated regions (UTRs) of mRNAs of iron related proteins. They can be in the 5´-UTR, which happens in the mRNA of FTL, FTH, and FPN, for example. But there are IREs in the 3'-UTR, for instance in the mRNAs of DMT-1 or TfR1. IRPs (iron regulatory proteins) are proteins that sense intracellular iron levels and interact with the IREs. When there is a lack of iron, IRPs bind to the respective IREs. If the IREs are in the 5'-UTR, the presence of the regulatory protein prevents the mRNA from being translated, and it is eventually degraded. Thus, when iron levels are low, FT and FPN are downregulated to prevent further storage or export of iron. Whereas, if the IREs are in the 3'-UTR, the binding of the IRP stabilizes the mRNA and allows it to be more extensively translated. Therefore, iron deficiency enhances DMT-1 and TfR1 synthesis, favouring cellular iron uptake. In case of elevated iron levels, IRPs either undergo a conformational change or are degraded, being unable to bind the IREs. Here, mRNAs of proteins like FT and FPN are free to be translated, being upregulated. On the other hand, the production of proteins like DMT-1 or TfR1 is decreased [7].

Additionally, iron metabolism is regulated at a transcriptional level. Hypoxia-inducible factors (HIFs) are transcription factors that are stabilized in hypoxic conditions and regulate the expression of various genes, including some that encode iron-related proteins, such as FPN [36], DMT-1 [37], and NCOA4 [38, 39].

2. The liver

2.1 Liver structure and cell types

The liver is a central organ in iron homeostasis. It is also responsible for a wide range of processes, such as hormone secretion, macronutrient metabolism, bile acid synthesis, detoxification, and immunity support, among others. The organ is anatomically divided into lobes [40] and functionally organized in lobules, which are hexagonal structures mainly composed of hepatocytes, alongside sinusoidal capillaries that radiate toward a central efferent vein. In each corner of the lobules, there is a portal triad composed of a bile duct, a portal vein, and a hepatic artery (Figure 3). The blood enters the liver through two sources, the portal vein and the hepatic artery, and exits the organ through hepatic veins that drain to the inferior vena cava [41].

Regarding cell types (Figure 3), the liver comprises five main different cell populations: hepatocytes, liver sinusoidal endothelial cells (LSECs), Kupffer cells (KCs), cholangiocytes, and hepatic stellate cells (HSCs).

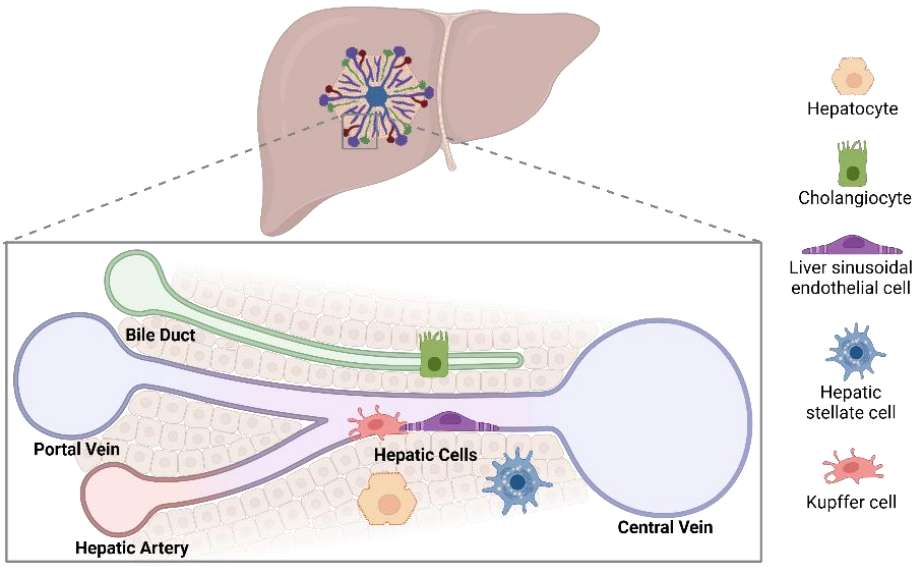


Figure 3 - The liver. The liver is represented, featuring a highlighted lobe. The microarchitecture of the lobe is illustrated with the central and portal veins, hepatic artery, bile duct, and hepatic cells amplified. Created with BioRender.com.

Hepatocytes are the most abundant cells in the liver, composing approximately 85% of the organ´s total mass [42]. Besides that, they are the liver primary functional cells, being responsible for xenobiotic detoxification [43], hepcidin secretion [22], nutrient metabolism [41], bile acid production [44], the synthesis of albumin, coagulation factors, acute phase proteins, and iron sequestering proteins [45], iron storage [3], and organ regeneration [46]. These cells are polarized, being close to the biliary system on one side and to

LSECs on the other. Hepatocyte polarity is crucial for their function, mainly regarding bile secretion and protein trafficking, and is maintained due to the interplay of cell-to-cell adhesion, cytoskeleton, extracellular matrix, and intracellular molecule trafficking [47].

LSECs are highly specialized endothelial cells (ECs) that form the wall of the liver sinusoids. These cells physically separate the inside of blood vessels from other hepatic cells, such as hepatocytes. LSECs are the large majority of the ECs in the liver, making up around 90% of all ECs present in the organ [48]. Concerning their morphology, LSECs present a discontinuous architecture as their luminal and abluminal membranes do not join at the cell junctions, but rather in places called *fenestrae*. Due to this discontinuous structure, LSECs are the most permeable cells in mammals, allowing the passage of small molecules from the blood vessels to the space of Disse (perisinusoidal space), but constraining the blood cells inside the vessels. The small molecules, including metabolites and pharmacological drugs, that reach the space of Disse may then be internalized by the hepatic cells. Of note, LSECs may also allow the passage of larger molecules such as lipoproteins [49], hormones [50], plasma proteins, and exosomes if they are capable of deforming through membrane pores. LSECs also perform transcytosis, which consists in the endocytosis of the molecules by the endothelial cells and posterior transference to the space of Disse [51]. Additionally, LSECs have a high endocytic capacity as well as a strong lysosomal activity, which allows them to clean waste from the blood and eliminate pathogens, showing their role in immunity [52]. LSECs not only contribute to liver homeostasis due to their barrier and cleaning function but also due to the crosstalk with other hepatic cells, as discussed below [53, 54].

The liver is the solid organ with the largest proportion of resident macrophages. For every 100 hepatocytes, there are 20 to 40 macrophages. It is thus logical to conclude that these cells play an important role in maintaining liver homeostasis. Liver resident macrophages are called Kupffer cells (KCs) and, in contrast with infiltrating macrophages, do not derive from monocytes, but rather from fetal liver monocytes [55]. KCs are located within the sinusoids throughout the liver and are crucial to eliminate pathogens from the blood, preventing them from entering the organ [56]. These cells are also involved in the removal of erythrocytes, hemoglobin-haptoglobin complexes, and vesicles containing hemoglobin, highlighting their role in iron metabolism [55].

Cholangiocytes represent a relatively small population of cells and line the bile ducts. They are responsible for bile maturation and transport and protect the biliary system from injury [57].

HSCs are resident mesenchymal cells located in the perisinusoidal space. These cells have two states, the quiescent and the activated one. In physiological conditions, HSCs remain in a quiescent state, characterized by the presence of lipid droplets that contain large amounts of vitamin A metabolites or retinoids. Upon liver injury, the quiescent HSCs become activated, mainly in response to oxidative stress and inflammatory signals. The activation of these cells entails an increase in their proliferation, differentiation into a myofibroblast-like cell, and production of extracellular matrix remodelling enzymes, among others. All these changes allow an increased production of extracellular matrix so that liver injuries may heal [58]. If HSC activation is excessive, it promotes the overproduction of collagen and other extracellular matrix components, leading to fibrotic tissue formation and ultimately resulting in liver fibrosis [59].

2.2 Intercellular communication in the liver

The regulation of iron homeostasis results from an interconnection of many factors and communication between different cells. Hepcidin production in the hepatocytes in response to iron levels provides a clear example of that. As described above, for hepatocytes to synthesize hepcidin, the BMP pathway must be activated by BMP6. BMP6 is produced by LSECs and, by paracrine communication, leads to hepcidin expression [54]. Up until recently, it was thought that LSECs directly sensed iron level variations and produced BMP6 in response. However, Colucci and colleagues demonstrated that augmented iron levels in LSECs were not sufficient to trigger BMP6 production. It was only when LSECs were co-cultured with hepatocytes or treated with the hepatocytes' supernatants that the iron overload induced BMP6 production. Thus, hepatocytes release an essential factor that triggers BMP6 production in the LSECs, which then leads to hepcidin expression back in the hepatocytes (Figure 4) [53].

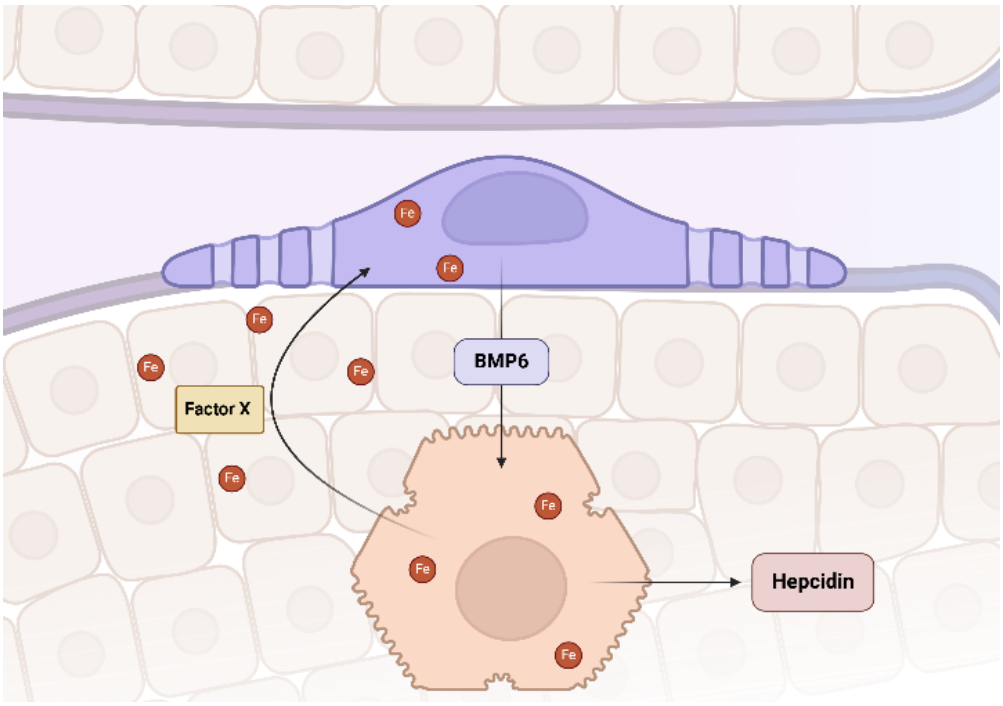


Figure 4 - Iron metabolism and intercellular communication in the liver. Upon an increase of hepatic iron, hepatocytes release an unknown factor (factor X) that promotes the synthesis of BMP6 by liver sinusoid endothelial cells (LSECs). BMP6 produced by LSECs triggers an intracellular signalling pathway in the hepatocytes that culminates in the production and secretion of hepcidin. Created with BioRender.com.

Besides the hepatocyte-LSEC axis, macrophages play a significant role in regulating liver homeostasis through intercellular communication. Many studies have demonstrated how factors released from macrophages, particularly in inflammatory conditions, impact hepatocytes (Figure 5). In addition to the role of IL-6 in hepcidin induction, other macrophage-derived cytokines, such as IL-1β, also modulate hepatocyte function in iron metabolism. Specifically, IL-1β promotes hepcidin production [60]. Furthermore, macrophages communicate with hepatocytes in various disease contexts. In the case of metabolic dysfunction-associated steatotic liver disease, pro-inflammatory macrophages release EVs containing pro-inflammatory cargo that promotes liver injury [61]. Additionally, in case of infection, macrophages release TNF-α and IL-1β, among others. Interestingly, it has been shown that these pro-inflammatory cytokines can trigger metabolic reprogramming in hepatocytes [62], as well as impact hepatocyte survival and NF-κB activation [63]. Another relevant aspect of the macrophage–hepatocyte communication is the induction of acute-phase protein production in hepatocytes, triggered by cytokines released from macrophages. This process will be further discussed later.

Although it is known that the intercellular communication in the liver is key to maintaining homeostasis and in inflammation contexts, there is still a long way to go when it comes

to understanding the mechanisms behind iron regulation and redistribution, particularly upon an intracellular infection.

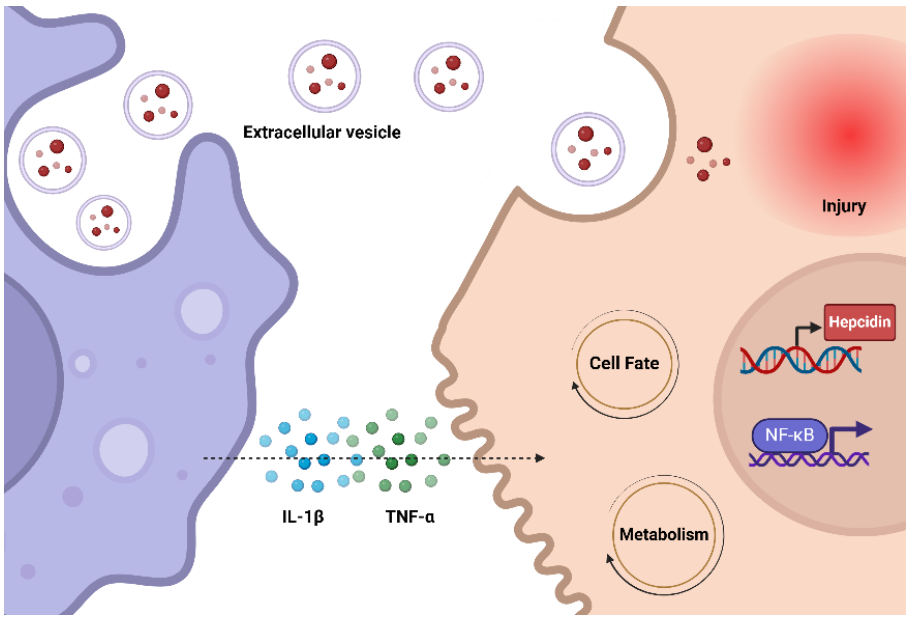


Figure 5 - Macrophage to hepatocyte communication. Macrophages can release extracellular vesicles with pro-inflammatory cargo that enhances liver injury. The phagocytes secrete IL-1β, which triggers hepcidin expression in hepatocytes. Additionally, upon infection, macrophages secrete IL-1β and TNF-α that trigger physiological changes in hepatocytes. These changes comprise metabolism reprogramming, cell survival alterations, and NF-κB activation. Created with BioRender.com.

3. Iron metabolism during inflammation

Macrophages recognize a variety of environmental stimuli and react to them, triggering an immune response. One of the stimuli that macrophages recognize is the presence of microbes. In this case, the immune cells have specific receptors, the pattern recognition receptors (PRRs), that bind to pathogen-associated molecular patterns (PAMPs) and lead to the initiation of a signalling pathway that culminates in the expression of different genes with the goal of protecting the organism from the pathogen. TLRs are an important class of PRRs present in macrophages. Their activation promotes the expression of pro-inflammatory cytokines, such as the tumor necrosis factor (TNF), among others [64]. Following TNF-α production, the cytokines are released and communicate in an autocrine way, intensifying the response in the same macrophage, and in a paracrine way, to initiate a response in neighbouring cells, helping to combat the infection [65, 66].

By recognizing the pathogens and initiating an immune response, macrophages influence iron-related gene expression in the liver. In this organ, pro-inflammatory cytokines, such as IL-6, IL-1, TNF-α, and IFN-γ trigger the production or decrease of acute phase proteins (APPs). APPs are proteins whose concentration in the serum

varies significantly with inflammation. If the pro-inflammatory cytokines cause their concentration to increase, they are considered positive APPs. Examples of positive iron-related APPs include hepcidin and ferritin [67]. Of note, serum ferritin is used a biomarker for inflammation [1]. On the other hand, negative APPs have decreased serum concentration upon inflammation. Transferrin is an example of an iron-related negative APP [67].

As stated before, IL-6 triggers hepcidin production and secretion. As the hormone inhibits iron absorption in the intestine and its release into circulation, its secretion is protective against extracellular pathogens. In contrast, transferrin's serum levels decrease upon inflammation, as cells take up more of this iron transporter protein [67].

Additionally, as inflammatory factors influence iron-related proteins, chronic inflammatory conditions induce diverse changes in the elements' metabolism. For example, upon metabolic dysfunction-associated steatotic liver disease, osteoarthritis, or chronic kidney disease it has been described that serum FT levels increase, iron accumulates in the synovial fluid and systemic iron levels drop, respectively [68-70].

At the intersection of iron metabolism and infection, macrophages appear as key players. These cells are not only crucial in innate immunity [71], but also central in iron metabolism [4]. Thus, it is worth mentioning how iron influences macrophage phenotype and vice-versa. Notably, iron status impacts macrophage polarization, the acquisition of a specific functional phenotype. Although this process is highly context-dependent, generally, when there is an iron overload in the phagocytes, they acquire an M1-like (pro-inflammatory) phenotype. On the other hand, in iron deficiency conditions, the cells polarize into M2-like (anti-inflammatory) macrophages. Macrophage phenotype also impacts their iron homeostasis. M1-like cells overexpress FT, having an iron sequestering behaviour, while M2-like macrophages overexpress FPN, releasing iron [72].

4. Iron metabolism deregulation during infection

4.1 Iron metabolism during infection

As mentioned above, most living organisms need iron to survive. Neither pathogens nor mammalian hosts are an exception. Thus, upon infection, there is a dispute for iron with bacteria trying to access the host´s nutrient and the host trying to starve the pathogen from it [20].

Bacteria have specialized molecules to scavenge iron. Examples of these molecules are siderophores, structurally diverse iron chelators that bacteria release to sequester and internalize iron [73].

Mammals also have mechanisms to starve the pathogens of the essential element, impairing their growth and ability to cause infection. As previously stated, upon infection, hepatocytes secrete hepcidin, which leads to a reduction of circulating iron levels. This decreases iron availability for bacteria [22]. Furthermore, there is a mechanism of FPN downregulation independent of hepcidin. The authors argue this might be the first line of defence to restrain pathogens' access to iron, protecting the host [28, 74]. However, hepcidin release and iron sequestration are not always advantageous for the host, nor a strategy used in every case. For instance, studies have shown that the absence of hepcidin in mice does not significantly impact *M. tuberculosis* growth [75]. Moreover, it has been seen that mice infected with *M. avium* and *M. tuberculosis* did not upregulate hepcidin [75, 76]. In addition, to show that iron sequestration is not always beneficial for the host, Chlosta and colleagues infected macrophages with *Salmonella*, an intracellular bacterium, and treated the cells with hepcidin. The authors verified that upon treatment with the hormone, bacterial growth augmented [77].

Besides hepcidin, other proteins make it harder for bacteria to acquire the host's iron. Proteins that bind the element in the serum decrease the nutrients' availability for extracellular pathogens to scavenge it. Examples of these proteins are haptoglobin and hemopexin, which bind to free hemoglobin and heme released from erythrocytes, respectively [78]. Lipocalin-2 also protects the host by impairing bacteria's iron acquisition. However, this protein binds iron-laden bacterial siderophores rather than the iron itself [79]. In the case of intracellular pathogens, natural resistance-associated macrophage protein 1 (NRAMP 1) is an important protein for host protection. In fact, mutations in its gene are linked to higher susceptibility to tuberculosis. NRAMP1 is a divalent metal transporter in the membrane of late endosomes or lysosomes that transports iron to the cytosol [80]. Intracellular pathogens, like *Mycobacteria*, resist inside the host cells' endosomes [81]. Thus, with NRAMP 1 transporting iron from the endosomes to the cytosol, bacteria will have less access to the nutrient [82].

4.2 Iron redistribution during Mycobacterial infection

M. avium are slow-growing non-tuberculous mycobacteria (NTM) that may cause opportunistic infections and colonize the intestinal and respiratory mucosa. There, they are phagocytosed by resident macrophages [81, 83] and resist digestion by blocking the maturation of the phagolysosome and preventing its acidification [81, 84]. In an attempt

to contain the infection, the host forms tissue granulomas [85]. These structures are clusters of infected macrophages, epithelial cells, and lymphocytes [85-87].

In a mouse model of intravenous infection, it was observed that iron accumulates inside these granulomas [88], as long as macrophages express FTH chains. FTH is essential for macrophage protection against iron-related damage [89], and its expression increases in macrophages upon *M. avium* infection, through the activation of TLR2 [90]. Furthermore, the levels of both subunits of FT are increased in the serum of *M. avium*-infected mice. Of note, serum FTH originates from macrophages, as this subunit is not augmented in the serum of mice with the FTH-coding gene knocked out in the myeloid lineage. Interestingly, in wild-type mice, *M. avium* infection leads to increased expression of FPN in hepatocytes, while in myeloid FTH-deficient mice, an increase in FPN expression is observed in macrophages and not in hepatocytes [91]. Additional studies are required to further characterize the intercellular communication that occurs in the granulomas to trigger these responses.

5. Cell cultures

In vitro models are essential tools in biological research, as they allow the study of cell-specific functions without the complexity of whole organisms. They are widely used to investigate metabolic and signalling pathways, cellular responses to stimuli, and cell–cell interactions. However, while their simplicity is advantageous, important biological relationships may be overlooked when relying on in vitro experiments. Thus, the choice of model should be made carefully, with the acknowledgment of both their advantages and limitations [92, 93].

These in vitro models often consist of cell cultures. Cell culture is usually defined as the maintenance of a monolayer of cells from a specific type under artificial conditions. Nevertheless, cultures are not limited to monolayers or single-cell types [93].

Cell cultures can be primary or immortalized. Primary cell cultures contain cells directly derived from tissues or organs of an organism. Eventually, primary cell cultures can be immortalized, meaning that they acquire the ability to proliferate indefinitely. This immortalization can happen spontaneously, as a consequence of the stress of the cells being moved to an artificial environment. This process may also be induced by controlled mutagenesis or cell transfection. Once primary cell cultures are immortalized, they become cell lines [92].

Primary cell cultures can be obtained from human tissue biopsies or from animal models, such as *Mus musculus,* through enzymatic treatments or mechanical methods to separate cells from their original tissues [94].

Moreover, cell cultures can be classified into three types according to the differentiation state of the cells. The first type involves stem cells, which are undifferentiated and able to originate any cell type [94]. As an example, cardiac fibroblasts can be obtained by the differentiation of pluripotent stem cells [95]. The second type comprises precursor cell cultures, in which the cells remain undifferentiated but are already committed to a specific lineage. An example of this type of culture is the bone marrow-derived macrophages, in which macrophage progenitor cells are isolated from the bone marrow of mice and cultured with macrophage colony-stimulating factor (M-CSF) to differentiate in vitro [96]. The third type includes fully differentiated cells. An example of this type is the isolation of hepatocytes from the liver of mice [97].

The use of primary cell cultures or cell lines has both advantages and disadvantages, which should be considered when selecting the appropriate system. Primary cell cultures retain key phenotypic and molecular characteristics, such as morphology and expression of surface and cytosolic markers, making them more representative of what is found in vivo and therefore more biologically relevant. While cell lines accumulate alterations in the genome, lose important characteristics of normal cells, and present low phenotype heterogeneity. On the other hand, primary cell cultures are often challenging to obtain, culture conditions need to be optimized, and they possess limited capacity for expansion. The yield of cell isolation may vary, and even the performance of the cells in culture may be more variable. Cell lines are easy to obtain, can propagate indefinitely, and usually have well-established optimal culture conditions [92, 98].

With all this in mind, for this project, we decided to use primary cell cultures, as our priority was the similarity to physiological conditions and biological relevance.

In order to study intercellular communication, the culture of one isolated cell type is not enough. Nonetheless, there are several methods to study paracrine communication in vitro.

One example of that is conditioned medium experiments. In these experiments, the supernatant of one cell culture is used as the medium for the other culture, allowing the study of the effects of molecules released by the first cell type in the second [53]. Although the different cell types are cultured independently, various communication factors of one cell type come into contact with the other. Another example is the use of

trans well inserts, where one cell type is cultured in the well of a plate and another in a permeable insert above it, allowing the exchange of several factors between the two populations without direct contact [61].

Additionally, there are more complex models that can mimic whole organs, such as organoids or organ-on-chips. Organoids are 3D multicellular structures that self-organize, simulating the architecture and function of organs in vitro [99]. Organ-on-chips are microfluidic devices in which cells are arranged in a way that reproduces the microarchitecture and dynamics of whole organs [100].

6. Thesis aims and structure

As discussed before, iron metabolism undergoes changes upon infection and inflammation [20, 22]. The mechanisms of communication between hepatic cells during these processes remain poorly understood. Thus, and due to the fact that the liver is a central organ in iron homeostasis [22], this project aims to identify the mechanisms of iron-related cross-talk between different liver cell types, particularly in inflammatory and infectious conditions. We decided to focus on three cell types: the macrophages, the hepatocytes, and the liver sinusoidal endothelial cells, because they are crucial in both the iron and inflammatory/ immune aspects [4, 45, 52, 53].

In order to study the cross-talk between these cells, we first needed to establish their primary cultures. We chose to use primary cultures as they better represent the cells in physiological conditions [92].

In summary, the specific aims of this MSc thesis are:

1. To establish the conditions for the culture of primary mouse macrophages, hepatocytes and liver sinusoid endothelial cells.
2. To characterize each of these cell types in terms of iron content and expression of iron-related proteins, in basal conditions.
3. To investigate the effects of external stimuli, namely iron overload, inflammatory stimuli, and *M. avium* infection in the previously characterized markers.
4. To investigate the mutual effects of one cell type on the other, in terms of iron regulation, using conditioned medium experiments and co-cultures.

Experiments aimed at the hepatocyte-macrophage communication were carried out at the Gomes' lab at i3S, Universidade do Porto. Experiments aimed at LSEC-hepatocyte communication were performed at the Muckenthaler lab, at University of Heidelberg.

Materials and Methods

Reagents

All reagents were purchased from Sigma-Aldrich (St. Louis, MO, USA), except if stated otherwise.

Primary mouse cells

Primary cells were obtained from 8- to 12-week-old or 22- to 26-week-old *Mus musculus* C57BL/6. The animals were kept in groups of five, inside ventilated cages with HEPA filters, and were fed with sterilized food and water *ad libitum*. The experiments were performed by people certified by the Federation for Laboratory Animal Science Associations (FELASA) and under the approval of Direção-Geral de Alimentação e Veterinária (DGAV) or Regierungspräsidium Karlsruhe (T-48/24).

Bone marrow-derived macrophages (BMM)

To obtain BMM, the bone marrow from the tibias and femurs of adult mice was flushed with Hank´s Balanced Salt Solution (HBSS) (GIBCO, Paisley, U.K.). Then, the cell suspension was centrifuged at 1200 rpm for 10 min, at 4 ºC, and the resulting pellet was resuspended in 4 mL of complete Dulbecco's Modified Eagle Medium (DMEM) (GIBCO, Paisley, U.K.) containing 10% fetal bovine serum (FBS). Afterwards, the suspension was transferred to a 6 cm diameter Nunclon Petri dish (Thermo Scientific, Meridian Rd., Rockford, IL 61101 U.S.A.) in 12 mL of complete DMEM plus 1.5 mL of L929 cell conditioned medium (LCCM), which contains M-CSF. The cells were incubated overnight at 37 ºC, 7% CO_2. After the incubation, the non-adherent cells were collected, and the plate was carefully washed with 10 mL of cold HBSS to ensure all cells were collected. The suspension was centrifuged at 1200 rpm for 10 min at 4 °C, and the pellet was resuspended in 4 mL of complete DMEM. Finally, the cell concentration was adjusted to 4 x 10^5 cells/mL. The cells were distributed on 24 or 6-well plates (Falcon®, Irvin, California, USA) and maintained in complete DMEM/10%LCCM. For cell culture maintenance, on the 4th day, 10% LCCM was added to each well, and on the 7th and 10th (for non-infected and non-treated cells) days, the medium was renewed.

In some experiments, after complete differentiation, macrophages were treated with 10 μM ferric ammonium citrate (FAC) in complete DMEM/ 10%LCCM for 24h.

BMM infection

Infection was performed with strain 25291 of *M. avium*, acquired from the American Type Culture Collection, Manassas, VA, USA. On the 10th day of culture, macrophages were infected with an *M. avium* 25291 suspension, with a multiplicity of infection of 2.5. The cells were incubated for 4 h at 37 °C, 7% CO_2. After the incubation, the cells were washed with warm HBSS four times to remove non-phagocytosed bacteria. Finally, DMEM/ 10%LCCM was added to the cells, and they were incubated at 37 ºC, 7% CO_2 for 48h.

BMM lysate and supernatant collection

After the infection or FAC treatment period, BMMs supernatant was collected for protein analysis. Supernatants were stored at -80 ºC before further analysis.

Cell lysates were collected for RNA extraction by adding 300 µL of the RNA extraction kit's lysis buffer (PureLink™ RNA Mini Kit, Invitrogen, Waltham, Massachusetts, USA) with 1% β-mercaptoethanol to the wells, resuspending the cells in the buffer, and collecting them. In the case of the collection of lysates for protein quantification, a lysis buffer composed of RIPA buffer (150 mM NaCl, 1.0% NP-40, 0.5% sodium deoxycholate, 0.1% SDS, 50 mM Tris, pH 8.0) with 1x protease inhibitor cocktail (PIC) (Roche, Basel, Switzerland) was used. After adding the lysis buffer, the wells were scraped with a cell scraper, and the suspension was collected. Lysates were stored at -80 ºC before further analysis.

Additionally, lysates were collected for intracellular iron quantification by adding phosphate buffered saline (PBS)/KCl with 5mM ethylenediaminetetraacetic acid (EDTA) to the wells, scraping them with a cell scraper, and collecting the suspension. After collection, cells were centrifuged at 2879 *g* for 10 min, the supernatant was discarded, and the pellet was dried, incubating it at 37ºC for 48h.

Plate collagen-coating

For hepatocyte and LSEC cultures, plates must be pre-coated with collagen, as these hepatic cells do not adhere to the plastic.

For the experiments in which hepatocytes were treated with FAC or co-cultured with BMMs, Type I bovine atelocollagen solution (Type I bovine atelocollagen solution, BICO, Gothenburg, Sweden) in PBS was used at a final concentration of 50 µg/mL. For the

coating itself, the collagen solution was added to each well of the plate, and it was incubated at 37 ºC for 2h.

For the culture of LSECs and for the experiments in which hepatocytes were cultured for the harvesting of conditioned media or treated with LSEC conditioned media, the coating was slightly different. To prepare the collagen solution, rat tail collagen type I (Life Technologies Corporation, Grand Island, NY, USA) was diluted to a final concentration of 50 µg/mL in 20 mM acetic acid. For the coating itself, the solution was added to each well of the plate, and the plate was incubated at room temperature for 1h.

In both cases, after incubation, the wells were washed twice with 1× PBS and the plate was allowed to air-dry. Once dry, plates were used immediately or stored at room temperature for short-term use.

Liver harvesting

In order to obtain primary hepatic cells, the liver of healthy *Mus musculus* was harvested.

For the experiments in which hepatocytes were treated with FAC or co-cultured with BMMs (performed at i3S, Porto), the organ harvesting was performed as follows. After euthanasia, the mice were dissected, and both the liver's inferior vena cava and portal vein were exposed. The inferior vena cava was cannulated with a 27G needle, and the liver was perfused with 20 mL of Perfusion Medium (17701038, GIBCO, Paisley, U.K.). Importantly, right after cannulation, the portal vein was cut. When there was only 5 mL of perfusion media left, the portal vein was clamped for approximately 15 sec. In sequence, the organ was perfused with 25 mL of Digestion Medium (17703034, GIBCO, Paisley, U.K.). When there was only 5 mL of digestion media left, the portal vein was clamped, once more, for approximately 15 sec. Of note, the media were kept at 37 ºC. Finally, the gall bladder was removed and discarded, and the liver was harvested. The organ was placed in a Falcon, on ice, containing 10 mL of digestion media.

For the culture of LSECs and for the experiments in which hepatocytes were cultured to collect conditioned media or treated with LSEC conditioned media (performed at University of Heidelberg), the procedure was similar, but with some adjustments in media compositions and volumes. The organ perfusion was performed with approximately 20 mL of Liver Perfusion Medium (17701038, GIBCO, Paisley, U.K.). The digestion was performed using 15 mL of Digestion Medium (HBSS, CaCl2, MgCl2, GIBCO, Paisley, U.K.) with HEPES solution (25 mM, BIOXTRA, 1 M, pH7.0-7.6) and 250 µL Liberase™

(1 mg/mL). Moreover, after harvesting the liver, it was placed in a tube with 15 mL of Hepatocyte Wash Medium (17704-024, GIBCO, Paisley, U.K.), on ice.

Primary hepatocyte (PH) culture

Following organ harvesting, we performed hepatocyte isolation.

For the experiments in which hepatocytes were treated with FAC or co-cultured with BMMs (performed at i3S, Porto), the procedure was as follows. The liver was placed with its media in a Petri dish, small incisions were made in the organ with a clamp, and it was pressed with a cell scrapper for the cells to be released. The cell suspension was filtered using a 70 µm cell strainer, and the dish was washed with 10 mL of complete William's media to recover every cell possible. Complete William's media is composed of the medium itself (GIBCO, Paisley, U.K.) with 200 mM L-glutamine, 4% FBS, and 1% Penicillin-Streptomycin (GIBCO, Paisley, U.K.). The cell suspension was again filtered with the strainer, and the cells were centrifuged at 50 *g*, 4 ºC for 2 min. The supernatant was discarded, the pellet resuspended in 10 mL of complete William's E media, and 10 mL of a solution of 60% Percoll™ (1.130 g/mL, Percoll™, 17-0891-02 Cytiva Sweden AB, Uppsala, Sweden) was added to the suspension. The cells were gently shaken and centrifuged at 200 *g*, 4 ºC for 10 min, and the pellet was resuspended in complete William's media. Another centrifugation was performed at 50 *g*, 4 ºC for 2 min. The pellet was again resuspended in William's media, and the cell concentration was adjusted to 2 x 10^5 cells/mL. Finally, the hepatocytes were plated in pre-collagen-coated 24- or 6-well plates and incubated at 37 ºC, 5% CO_2. After 3h, cells were washed twice with PBS 1x, the media was changed, and cells were incubated overnight.

For the experiments in which hepatocytes were cultured for the harvesting of conditioned media or treated with LSEC conditioned media (performed at the University of Heidelberg), the procedure was as follows. The liver was transferred along with the wash medium to a Petri dish. Then, the organ was decapsulated, and cells were liberated by making small incisions and agitating the organ. The cell suspension was filtered with a 100 µm strainer, followed by a 70 µm strainer, to remove larger debris. To maximize cell recovery, the Petri dish was rinsed with an additional 20 mL of Hepatocyte Wash Medium, and all remaining cells were filtered as described before. The cell suspension was centrifuged at 4 ºC, 50 *g* for 2 min, the pellet was resuspended in 20 mL of cold PBS, and the centrifugation was repeated. Then, the pellet was resuspended in warm complete William's E media. Complete William's E media consists of the medium itself

with GlutaMAX™ (GIBCO, Paisley, U.K.), 4% FBS, and 1% Penicillin-Streptomycin (P4333-100ML). Then, cells were counted and plated at a density of 2.2 x 10^5 cells/well. After a 3h incubation period, cells were washed and the medium was changed, as detailed above.

For some experiments, the day after cell plating, the hepatocytes were treated with a solution of 1, 10, 25, 50, or 100 μM FAC for 24h or a solution of 10 ng/mL LPS for 48h.

PH and BMM co-culture

In order to co-culture primary hepatocytes and BMM, trans-well inserts were used. In this system, hepatocytes are cultured on collagen pre-coated 6-well plates, and macrophages are cultured in trans-well inserts. Once both cell types are ready, the inserts are placed on top of the wells, and the cells exchange soluble factors without direct contact.

Firstly, BMMs were obtained as described above. In this case, the macrophage progenitor cells were plated in the inserts (cellQART®, 6-well cell culture insert 0.4 µm PET clear, SABEU GmbH, Germany) and the inserts were placed in 6-well plates. The culture was maintained as previously described. On the 10th day of culture, macrophages were infected as described above.

On the day of BMM infection, hepatocytes were isolated and plated in 6-well plates, as explained before. 3h after hepatocyte plating, fresh medium was added to the hepatocytes, and the inserts with the non-infected or infected macrophages (after non-phagocytosed bacteria removal) were placed on top of the hepatocyte wells. Cells were incubated for 60h at 37 ºC, 5% CO_2.

Collection of PH lysates and conditioned media

After the FAC treatment period, PHs supernatants were collected for protein analysis, and cell lysates for RNA extraction, as well as for protein and iron quantification. The collection was performed following the protocol used for the collection of BMM supernatants and lysates.

After co-culture with BMM, PH lysates for RNA extraction were also collected following the previously described protocol.

For the preparation of conditioned media, after collection, the culture supernatants were centrifuged at 4 ºC, 400 *g* for 10 min, and the supernatants were collected. These were centrifuged again at 4 ºC, 2000 *g* for 10 min. Finally, the supernatants from this last centrifugation were collected and stored at -80 ºC before further use.

LSEC culture

Primary LSEC were obtained from the liver of 22 to 26-week-old *Mus musculus*. After the organ harvest, similarly to what was performed for hepatocyte isolation, the liver and the Wash Media were transferred to a Petri dish. The organ was decapsulated, and the cells were filtered with 100 and 70 µm strainers. Then, 20 mL of Hepatocyte Wash Medium was added to the dish, and the liver was pipetted up and down multiple times with a serological pipette. This is done to further break down the tissue and facilitate cell release. The plate was washed, and all remaining cells were filtered with the strainers.

The tubes were centrifuged at 4 °C, 50 *g* for 5 min, the supernatant was recovered, and the pellet was resuspended in 20 mL of cold PBS. Afterwards, both the supernatant and the resuspended pellet were centrifuged under the same conditions supernatants were recovered. Then, we performed another centrifugation of the supernatants at 4 °C, 400 *g* for 10 min, and kept the pellet.

Following this, a density gradient centrifugation was performed. Thus, each pellet was resuspended in 1 mL of 17.6% OptiPrep (STEMCELL Technologies, Vancouver, Canada), and the volume was adjusted to 5 mL. Then, 5 mL of 8.2% OptiPrep were loaded on top of the more concentrated solution, and 2 mL of B-PBS (1 mg/ml bovine serum albumin (BSA) solution in PBS) were loaded, as well, on top of the less concentrated OptiPrep. The tubes were centrifuged at 14000 *g* with no brake for 17 min. The 3 mL of the top layer were discarded, and the cells present in the fraction between the two OptiPrep solutions were collected.

Cells were resuspended in 10 mL B-PBS and centrifuged at 4 ºC, 1400 *g* for 10 min. Then, the pellet was dried and resuspended it in complete William's E with vascular endothelial growth factor (VEGF) (1:10000, PeproTech, Rocky Hil). Following the resuspension, cells were placed in a well of a 6-well plate and incubated at 37 ºC for 12 min. After the incubation, the cell suspension was transferred to a new well. Additionally, the previous well was washed with complete William's E media with VEGF, and the suspension was transferred to the new well. Cells were incubated in the same conditions. Then, the suspension was collected to a Falcon tube and the same wash was performed.

Finally, the cells were counted and plated with a density of 10^6 cells/well. Cells were incubated at 37ºC, 5% CO_2 for 3h, and at the end of the incubation period, they were washed two times with PBS 1x, fresh media was added, and cells were placed in the incubator overnight.

LSEC treatment

Conditioned media and iron

The day after LSEC isolation, cells were treated with hepatocyte conditioned media and Ferric nitrilotriacetic acid (FeNTA). Cells were kept in the following conditions: starvation media (William's E with GlutaMAX™, Penicillin-Streptomycin and VEGF), starvation medium and FeNTA, conditioned media, or conditioned media and FeNTA. For the treatment, cells were washed twice with 1x PBS. Then, either 500 µL of starvation or conditioned media was added to each well of the 24-well plate. The cells were incubated for 1h at 37 ºC, 5% CO_2. Following this incubation, 2.5 µL of FeNTA 50 µM was added to each well, and the cells were incubated for 6h in the same conditions.

TNF-α and Fibroblast-Stimulating Lipopeptide-1(FSL-1)

The day after cell isolation, LSEC were washed twice with PBS 1x and fresh complete William's E media with VEGF was added, alongside 10 ng/mL of TNF-α (Recombinant Mouse TNFα Lyophilized, Invitrogen, Waltham, Massachusetts, USA) or 100 ng/mL of FSL-1 (InvivoGen, San Diego, California, USA). Control cells received complete William's E media or complete William's E media and VEGF. The cells were incubated for 24h. For the collection of stimulated LSECs' conditioned media for the analysis of its effects on the intercellular communication, the day after LSEC isolation, cells were washed and treated as described above. In this case, the treatment lasted 6h. Afterwards, cells were washed and fresh complete William's E media with VEGF was added. Finally, LSEC were incubated overnight.

LSEC collection

After the treatment, LSEC supernatant was collected for protein analysis using the procedure by which BMM supernatants were collected.

Cell lysates for RNA extraction were also harvested. The cells were washed twice with PBS before the lysis. Then, 400 µL of lysis buffer (Bio&Sell's RNA extraction kit) was added to each well, and the plate was stored at -20 ºC until further use.

Additionally, cells were collected for intracellular iron quantification. In this case, after the washes with PBS, 500 µL of accutase solution (400-600 units/mL) was added to each well, and the cells were incubated at 37 ºC for 10 min. Following the incubation, 500 µL of Williams E media with FBS was added to each well, and they were scraped. The cell suspension was collected and centrifuged at 400 *g*, 4 ºC for 10 min. The supernatant was discarded, the pellet was washed with 500 µL of buffer (PBS/KCl EDTA 5 mM), and the cells were centrifuged again. Then, the supernatant was discarded, and the pellets were frozen with liquid N_2, and stored at -80 ºC.

Finally, the pellets were thawed and dried as described before.

LSEC's conditioned media collection

In order to study the effects of TNF-α and FSL-1 on the communication between LSEC and hepatocytes, LSEC conditioned medium was collected. Following the treatments and overnight incubation with fresh William's E media, LSEC's supernatant was collected and centrifuged at 400 *g*, 4 ºC for 10 min. After the first centrifugation, the supernatant was collected and centrifuged at 2000 *g*, 4 ºC for 10 min. Finally, the supernatant from the last centrifugation was collected and stored at -80 ºC until further use.

PH treatment with LSEC conditioned media and cell collection

Hepatocytes were treated with LSEC conditioned media. The day after hepatocyte isolation, the cells were washed twice with PBS 1x, and LSEC conditioned media (from untreated cells or cells stimulated with TNF-α and FSL-1) was added to each well. Moreover, William's E (supplemented with GlutaMAX^{TM}, Penicillin-Streptomycin, and FBS) media with or without VEGF were added, as controls. Then, cells were incubated at 37 ºC for 6h.

After the treatment, the cell lysates were harvested for PCR. Cells were washed twice with PBS 1x before lysis. Then, 400 µL of lysis buffer (Bio&Sell's RNA extraction kit) was added to each well, and the plate was stored at -20 ºC until further use.

Viability assay

In order to determine hepatocyte viability, a resazurin viability assay was performed. Firstly, a solution of 1.5 mM of resazurin in PBS was prepared and filtered. Of note, the

compound was always protected from the light. After 24h of each specific treatment, the resazurin solution was added to the hepatocytes in a volume corresponding to 10% of the total culture medium volume. Hepatocytes were incubated with resazurin for 6h, and the fluorescence of resorufin was measured, with an excitation wavelength of 530 nm and an emission wavelength of 590 nm.

Fluorescence-activated Cell Sorting (FACS)

In order to verify the purity of the LSEC population, the cells were analysed by FACS. After 24h of culture, 250 μL of accutase solution (400-600 units/mL) was added to each well of the 24-well plate, and the cells were incubated at 37 ºC for 15 min, which allowed them to detach from the plate. After the incubation, 250 μL of FACS buffer (50mL PBS, 1 mL FBS, 250 μL EDTA pH8 0.5M) was added to each well. Then, the wells were gently scraped, and the cells were harvested.

Cells were centrifuged at 400 *g*, 4 ºC for 10 min, and the supernatant was discarded. Then, the pellet was resuspended in 90 μL of FACS buffer and 10 μL of FcR blocking reagent (1:10, Miltenyi Biotec). For blocking, cells were incubated at 4ºC for 10 min. After the incubation, the cells were divided into two tubes. One tube was used for unstained cells analysis. To the other tube, the antibodies mix was added. The antibodies used were anti-CD146 coupled with phycoerythrin (PE) (1:100, Biolegend, San Diego, CA, USA), anti-stabilin-2 coupled with fluorescein (FITC) (1:100, Biozol Diagnostics Vertrieb GmbH, Hamburg, Germany), and anti-F4/80 coupled with allophycocyanin (APC) (1:100, Biolegend, San Diego, CA, USA). After the addition of the mix, cells were incubated on ice, in the dark, for 30 min. Then, cells were centrifuged at 400g, 4 ºC for 10 min, the supernatant was discarded, and the pellet was resuspended in 300 μL of FACS buffer. The centrifugation was repeated, and the pellet was again resuspended in 300 μL of FACS buffer. The unstained cells group was divided, and to one of the tubes DAPI (1:1000, DAPI and Hoechst Nucleic Acid Stains, Thermo Fisher Scientific, Waltham, Massachusetts, USA) was added. Unstained cells were analysed to measure autofluorescence and calibrate the machine, cells were stained with DAPI to infer about cell viability, and cells were stained with the different fluorophore-conjugated antibodies for their characterization. The fluorescence measurements were performed using the CYTEK AURORA (Cytek Biosciences, Fremont, CA, USA).

Supernatant concentration

The supernatants were concentrated to improve protein detection.

For the concentration of BMM and hepatocyte samples, filter tubes (Amicon® Ultra-15 Centrifugal Filter Devices) were used. Before use, the tubes were rinsed in water to eliminate any residues. After this wash, the supernatants were placed in the tubes and centrifuged at 4000 *g* and 4 °C for 1h. The supernatants were resuspended every 10 min to avoid filter clogging.

For the concentration of LSEC samples, as well as DMEM and William's E media, other filter tubes (Amicon® Ultra-0.5 Centrifugal Filter Devices) were used. In this case, 500 µL of the samples were placed in each tube, and they were centrifuged at 14000 *g* and 4 °C for 15 min. Then, the filters were placed upside down inside a collection tube and centrifuged at 1000 *g* and 4 °C for 2 min. This process was repeated until the whole samples were concentrated.

After the concentration, the concentrates were stored at -80 ºC.

Protein quantification

The protein in the supernatant concentrates was quantified using the NanoDrop™ One (Thermo Fisher Scientific, Waltham, Massachusetts, USA).

For protein quantification in cell lysates, the Pierce™ BCA Protein Assay Kit (Thermo Fisher Scientific, Waltham, Massachusetts, USA) was used. Before starting the kit, the cells were pipetted up and down, kept in ice for 30 min, and, finally, centrifuged at 14000 g, at 4 ºC for 10 min. After the centrifugation, the supernatant was collected, and the kit's protocol began.

Firstly, the bovine serum albumin (BSA) standards were prepared. The standards were obtained by diluting a solution of BSA 2 mg/mL with lysis buffer. The standards' range of concentrations was from 2 to 0.025 µg/mL. Then, 25 µL of the standards and samples were added to each well of a 96-well plate, along with 200 µL of the working solution (mixture of the kit's reagents A and B in a ratio of 50:1, Reagent A:B). The plate was agitated for 30 s and incubated at 37 ºC for 30 min. Finally, the absorbance at 562 nm was measured, and the total concentration of protein in the samples was determined.

Western blot

A western blot was performed to assess the presence of EV markers and verify the presence of FTL and FTH in the supernatant concentrates of infected, non-infected, and FAC-treated macrophages, as well as in the supernatant concentrates of FAC-treated and non-treated hepatocytes.

Firstly, the gels were prepared by the polymerization of a 10% SDS-polyacrylamide gel followed by the polymerization of the stacking gel.

Afterward, the samples were prepared by adding 10 µg of protein, 4x Laemmli buffer (Bio-Rad, Hercules, CA, USA) with 10% β-mercaptoethanol, and water to achieve a total volume of 30 µL. The samples were heated at 90ºC for 5 min to denature the proteins. The denatured samples were loaded onto the gel, and the electrophoresis was ran at 30 mA per gel for approximately 1 h.

Following the electrophoresis, the proteins were transferred from the gel to a PVDF membrane at 90 V, 4ºC for 90 minutes. Before the transfer, the membranes were activated with methanol for 10 sec, water for 5 min, and transfer buffer (14.5 g/L glycine, 3 g/L Tris base, 0.05% SDS 10%, 20% methanol) for 15 min. During the procedure, the membranes and gels were kept in transfer buffer. After the transfer, the membranes were stained with Ponceau S to check the protein content and to cut the membrane, selecting the parts containing the proteins of interest.

Then, the membrane was blocked with 5% BSA in Tris Buffered Saline with Tween 20 (TBS-T) (NaCl 150 mM, Tris-HCl pH 7.4 20 mM, Tween 20 0.1% in 1 L of deionized water) for 1-2 h at room temperature (RT). After blocking, the membrane was washed twice with TBS-T for 10 min each time. Afterward, the membrane was incubated overnight at 4ºC with an antibody against FTL (1:1000, Abcam, Cambridge, United Kingdom), FTH1 (1:1000, Cell Signalling Technology, Inc., Danvers, Massachusetts, United States), or CD63 (1:1000, Santa Cruz Biotechnology).

After incubation, the membranes were washed three times with TBS-T, for 5 minutes each time, and incubated with a secondary antibody conjugated with horseradish peroxidase (1:10000, The Binding Site, Birmingham, UK) for 1h. The membrane was washed three more times for 5 min each. Afterward, the enzyme-substrate (Clarity™ Western ECL Substrate, Bio-Rad, Hercules, CA, USA) was added and images of the membranes were obtained using a ChemiDoc (Bio-Rad, Hercules, CA, USA).

Enzyme-linked immunosorbent assay (ELISA)

To assess the presence of FTL and FTH in the concentrates of BMM, PH, and LSEC supernatants and cell lysates, a homemade sandwich ELISA was performed based on antibodies kindly provided by Paolo Santambrogio and Sonia Levi, Università Vita-Salute San Raffaele, Milano.

Firstly, BMM and PH supernatants were diluted 10 times, and the cell lysates were diluted 2 times in PBS with 1% BSA. A 96-well plate was coated with 100 µL of capture antibodies (8 µg/mL) per well and incubated at 4 ºC overnight. After incubation, the wells were washed 4 times with a washing buffer (PBS with 0.05% Tween 20). Then, the plate was blocked with 100 µL of a blocking solution (PBS with 2% BSA) per well and incubated for 1h at room temperature. Afterward, one wash was performed with the designated buffer.

Then, 100 µL of the samples was added to each well, along with the standards (0 to 400 ng/mL for FTH and 0 to 20 ng/mL for FTL), and the plate was incubated for 2h at RT. Then, the wells were washed 4 times. Afterward, 100 µL of detection antibodies (4 µg/mL) was added to each well, the plate was incubated for 1h at RT, and the wells were washed 4 times. Then, 100 µL of the enzyme (1:4000, avidin-HPR) was added to each well and the plate was incubated for 1h at RT, followed by 4 washes. After this, 100 µL of substrate (1x TMB Substrate Solution, Invitrogen, Massachusetts, USA) was added to each well and the plate was incubated for 10 minutes at RT, in the dark. Finally, 100 µL of stop solution was added to each well, and the absorbance was measured at 570 and 450 nm. The final absorbance values were obtained by subtracting the values from the read at 570 nm from the ones at 450 nm. Ferritin concentrations were interpolated from the standard curve using a four-parameter logistic fit. The absorbance of the buffer used to dilute the standards and samples was considered. To determine the concentrations of FTH and FTL in the supernatants, both the sample dilutions and the supernatant concentrations were taken into consideration. For fold-change analyses, ferritin subunit concentrations were normalized to the total protein concentration. Fold change in untreated samples was calculated relative to the mean concentration of all untreated samples, whereas fold change in treated samples was calculated relative to the concentration of ferritin in the corresponding untreated sample from the same independent experiment.

RNA extraction

RNA was extracted from BMM and hepatocytes lysates using an RNA extraction kit (PureLink™ RNA Mini Kit, Invitrogen, Waltham, Massachusetts, USA). Every sample was homogenized using a rotor-stator homogenizer for approximately 45 sec and centrifuged at 2400 *g* for 5 min. The supernatant was collected and transferred to a new RNase-free tube. 70% ethanol was added to each sample (1 equal part of ethanol), the mix was vortexed and transferred to a kit's column 700 µL at a time. The samples were centrifuged at 12000 *g* for 15 sec, and the filtrate was discarded. This procedure was repeated until the entire sample was processed. Then, the wash buffer I was added to the column, centrifuged at 12000 *g* for 15 sec, and the filtrate was discarded. Afterward, the buffer II was added to the column, centrifuged at 12000 *g* for 15 sec, and the filtrate was discarded. The wash was repeated with wash buffer II, and the tubes were centrifuged again with no buffer at 12000 *g* for 1 min. Then, the columns were placed in a collection tube, 30 µL of RNase-free water was added to the columns, and they were incubated for 1 min. The tubes were centrifuged at 12000 g for 2 min, obtaining the RNA in the collection tube. The filtrates containing the RNA were kept on ice, and the RNA concentration was measured using the NanoDrop One Spectrophotometer (Thermo Scientific, Waltham, Massachusetts, USA).

RNA extraction from the LSEC lysates was performed with another RNA extraction kit (Bio&Sell). The lysate was placed in an E spin filter and centrifuged at 10000 *g* for 2 min. Then, 400 µL of 70% ethanol was added to the filtrate. The mixture was transferred to a S spin filter and this was centrifuged at 10000 *g* for 2 min. The filtrate was discarded, the washing solution IT was added to the filter, and it was centrifuged again at 10000 *g* for 1 min. This step was repeated with the washing solution MT. Following the washes, the filtrates were discarded, and the filters were centrifuged for 2 min to dry. Finally, 25 µL of RNase-free water was added to each filter and they were centrifuged at 6000 *g* for 2 min. The filtrates containing the RNA were kept on ice, and the RNA concentration was measured using the NanoDrop 2000 Spectrophotometer (Thermo Scientific, Waltham, Massachusetts, USA).

cDNA synthesis

cDNA was synthesized from the extracted RNA to then perform a qRT-PCR.

In case of samples from macrophages and hepatocytes, the NZY First-Strand cDNA Synthesis Kit (NZYtech, Lisboa, Portugal) was used. A mix with water, the reverse

transcriptase, and the master mix was added to the RNA as instructed by the manufacturer. Then, the samples were placed in a Thermocycler (Bio-Rad Laboratories, Hercules, California, United States) and incubated at 25 ºC for 10 min, 55 ºC for 30 min, and 85 ºC for 5 min. Afterwards, the samples were chilled at 4 ºC and 1 µL of RNase was added to the samples. Finally, the samples were placed in a Thermocycler for 20 min at 37 ºC. The cDNA was stored at -20 ºC until further use.

In case of samples from LSECs, water was added to all the samples to obtain the same concentration and volume for everyone. Then, random primers (1:25, Life Technologies, USA 48190-011) were added to the mixture and it was incubated at 72 ºC for 10 min, followed by a cooling period of 2 min on ice. A mixture of deoxynucleotide triphosphate (DNTPs) (1:25, Life Technologies, USA R0193), reverse transcriptase (1:50, RevertAid H Minus, Life Technologies, USA EP0452), and a buffer (1:5, 5X Buffer, Maxima First Strand cDNA Synthesis Kit, Life Technologies) was added to each sample. The mixture was incubated for 90 min at 42 ºC and for 10 min at 72 ºC. The cDNA was stored at -20 ºC until further use.

Quantitative Real Time (qRT) -PCR

To quantify gene expression, a qRT-PCR was performed.

In case of samples from macrophages and hepatocytes, the gene Hypoxanthine-guanine phosphoribosyl transferase (*Hprt1*) was used as the reference gene. The protocol began with the reaction mixture preparation, in which the reverse and forward primers (1:20), the enzyme and fluorophore mixture (1:2, iTaq Universal SYBR Green – Bio-Rad Laboratories, Hercules, California, United States) was mixed alongside water to obtain 19 µL of mixture per sample. Primer sequences are listed in Table 1. Regarding *Fth1* analysis, after the mixture preparation, 1 µL of cDNA was added to each well of a 96-well plate, followed by 19 µL of the reaction mixture. For the rest of the genes, 1 µL of cDNA was added to a 384-well plate, followed by 9 µL of the reaction mixture. In both cases, the plate was centrifuged at 1000 *g* for 1 min. Then, the qPCR was ran on IQ5 (Bio-Rad Laboratories, Hercules, California, United States). During the first stage of the protocol, the samples were heated for 5 min at 94 ºC. Afterwards, there is a stage that is repeated 24 times. This stage consists of 30 seconds at 94 ºC, 1 min at 30 ºC, and 30 sec at 72 ºC. At the end of the cycles, the samples were heated for 5 minutes at 72 ºC and kept at 4 ºC. The cycle threshold (Ct) values were obtained for each sample with the Bio-Rad Laboratories iQTM5 software.

Table 1 - List of primers' sequences used with BMM and PH samples.

Gene	Forward primer sequence	Reverse primer sequence
Hprt1	5'-GGTGGAGATGATCTCTCAAC-3'	5'-TCATTATAGTCAAGGGCATATCC-3'
Fth1	5'-GCTGAATGCAATGGAGTGTGCA-3'	5'-GGCACCCATCTTGCGTAAGTTG-3'
Ftl	5'-ACCTACCTCTCTCTGGGCTT-3'	5'-TGGCTTCTGCACATCCTGGA-3'
Bmp6	5'-TCCCCACATCAACGACACCA-3'	5'-TCCCCACCACACAGTCCTTG-3'
Fpn	5'-TTGGTGACTGGGTGGATAAGAATGC-3'	5'-GCGAGAGGATGACGGACACATTC-3'
Tfr	5'-GCAGCATTGGTCAAAACATGC-3'	5'-GCTTTGGGCATTTGCAACCC-3'

For LSEC samples, the same housekeeping gene was used as a reference. For the qRT-PCR, firstly, a mixture 10 mM forward and reverse primers for the target gene *Bmp6* and for the housekeeping gene *Hprt1* was prepared. Primer sequences are listed in Table 2. Then, the reaction mixture was prepared by the addition of water, the primers (0.5 mM), and the Sybr Green mix (1:1, Applied Biosystems, Waltham, Massachusetts, USA). After reagents preparation, 5 µL of each sample was added to the wells of the PCR plate, along with15 µL of the mixture. The plate was centrifuged at 1000 *g* for 1 min. Then PCR was ran. The first stage is a 7 min incubation at 95 ºC, the second stage is composed of 15 sec at 95 ºC and 1 min at 60 ºC and is repeated 40 times. During the melting curve phase, firstly, the temperature is 95 ºC for 15 sec, then 60 ºC for 1h, and finally, 95 ºC for 20 sec. Ct values were obtained for each sample using StepOne software.

Table 2 - List of primers' sequences used with LSEC samples.

Gene	Forward primer sequence	Reverse primer sequence
Hprt1	5'-TCCTCCTCAGACCGCTTTT-3'	5'-CCTGGTTCATCGCTAATC-3'
Bmp6	5'-ATGGCAGGACTGGATCATTGC-3'	5'-CCATCACAGTAGTTGGCAGCG-3'

ΔCt (equation 1) and $\Delta\Delta$Ct (equation 3), as well as the relative expression (equation 2) and fold change (equation 4), were calculated respecting the equations below.

$$1)\ \Delta Ct = Ct_{target\ gene} - Ct_{housekeeping\ gene}$$

$$2)\ Relative\ expression = 2^{-\Delta Ct}$$

$$3)\ \Delta\Delta Ct = \Delta Ct_{sample} - \Delta Ct_{control}$$

$$4)\ Fold\ change = 2^{-\Delta\Delta Ct}$$

Intracellular iron quantification

Iron intracellular quantification was performed by our collaborator Professor Agostinho Almeida (Faculty of Pharmacy, University of Porto), through atomic absorption spectrometry, as previously described by Mesquita and colleagues [89].

Statistical analysis

Data were analysed with GraphPad Prism 9.4 program (GraphPad Soft-ware, Inc., La Jolla, CA, USA). Data are expressed as means + standard deviation. The number of samples is indicated in the legend of each figure. Comparisons between groups were performed by using an ordinary one-way ANOVA or t-test, and the p-value was determined. The differences between groups were considered significant when the p-value was lower than 0.05.

Results

1. Optimization of primary cell cultures

The general aim of this thesis is to identify the mechanisms of iron-related cross-talk between macrophages, hepatocytes, and LSEC, particularly under inflammatory and infectious conditions. In order to study these mechanisms, we established primary cell cultures, which was the first task of this project.

1.1 BMM culture

There is a very well-established protocol for bone marrow-derived macrophage culture in Gomes' lab, which we followed to obtain primary macrophages.

As shown in Figure 6, macrophage progenitor cells isolated from the bone marrow of mouse tibiae and femurs were plated on day 0 of culture. These progenitor cells were small and round but started to acquire a more elongated shape as the culture progressed. On the 10th day of culture, the majority of the cells in culture had acquired this shape, characteristic of differentiated macrophages.

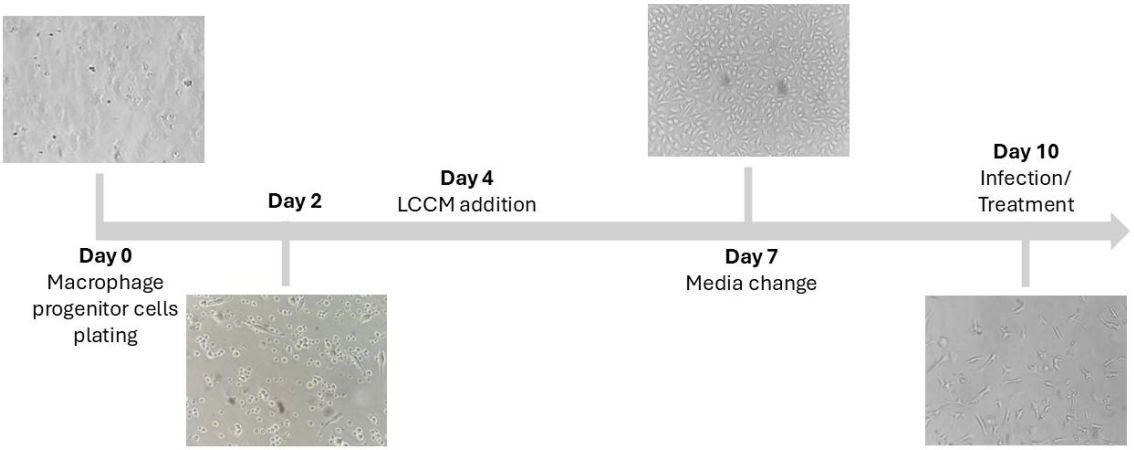


Figure 6 - Timeline for bone marrow-derived macrophages culture maintenance. Light microscope images, with a 200x magnification, of BMM on day 0, 2, 7, and 10 of culture. BMMs were cultured by obtaining the macrophage progenitor cells from the bone marrow of the tibia and femur of mice. The progenitor cells were plated and maintained in complete DMEM with 10% LCCM. On the 4th day of culture, 10% LCCM was added to the medium. On the 7th day, the medium was renewed, and on the 10th day, the macrophages were fully differentiated and ready for infection or other treatment.

1.2 Primary hepatocyte culture

Primary hepatocytes were directly isolated from mice's livers. As shown in Figure 7, adherent hepatocytes, the day after isolation, already displayed the characteristic morphology of these hepatic cells. They were larger, had a more cuboidal shape, and

contained multiple nuclei. In addition to the adherent hepatocytes, some small round cells were observed in suspension, which will afterwards be discarded by washing.

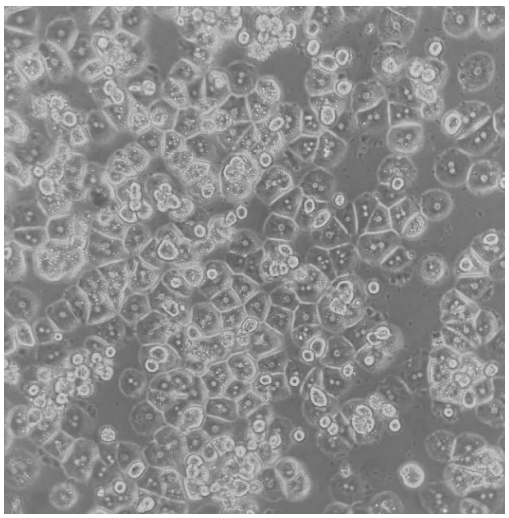


Figure 7 - Primary hepatocyte culture. Light microscope image, with a 400x magnification, of the primary hepatocyte culture, the day after isolation. Hepatocytes were obtained through their isolation from mice's liver. Cells were maintained in complete William's E media. The day after isolation, cells were ready for additional treatments.

Besides optimizing the conditions for hepatocyte harvesting and culturing, we decided to evaluate the effect of iron overload in the viability of cultured primary hepatocytes. We treated the cells with various concentrations of FAC for 24h and performed a viability assay with resazurin. Resazurin is metabolized by viable cells into resorufin, a fluorescent compound. Consequently, fluorescence correlates positively with cell viability. As demonstrated in Figure 8, there were no significant changes in fluorescence emission upon FAC treatment. Thus, hepatocyte viability was not impaired when they were treated with FAC, up to 100 micromolar.

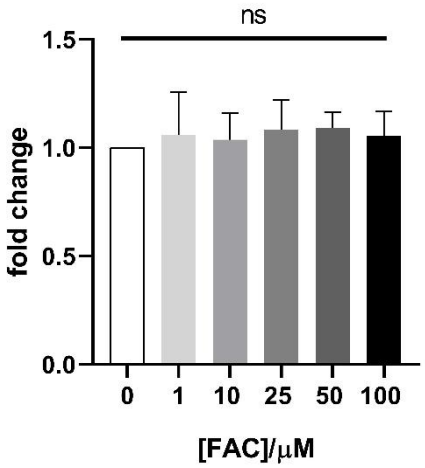


Figure 8 - Ferric Ammonium Citrate (FAC) does not alter hepatocyte viability. Primary hepatocytes were treated with 0, 1, 10, 25, 50 or 100 μM of FAC for 24h. For the viability assay, cells were exposed to 0.15 mM of resazurin and incubated

for 6h at 37 ºC. After the incubation period, fluorescence was measured. $\lambda_{excitation}$ was 530 nm, and $\lambda_{emission}$ was 590 nm. Each bar represents the mean + standard deviation fold change (relative to untreated cells) of two independent experiments. Each symbol represents the mean of three technical replicates. Statistics: One-way ANOVA.

In Muckenthaler's lab, we optimized the culture of primary LSECs. Similar to the hepatocyte protocol, LSECs were directly isolated from mice livers. Morphologically, cultured LSECs were small and rounded, often displaying elongated extremities (Figure 9).

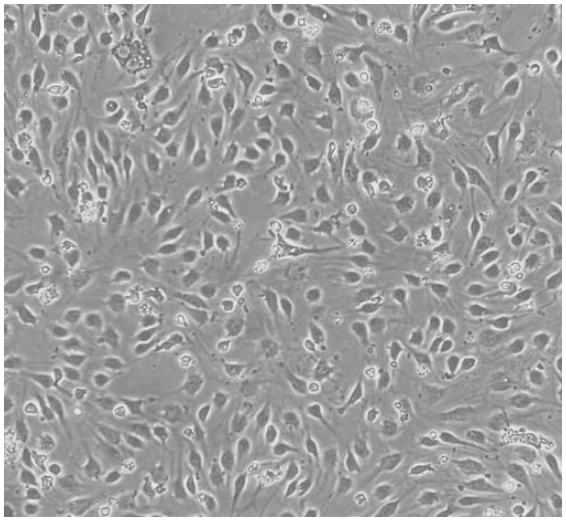


Figure 9 - Primary liver sinusoidal endothelial cell (LSEC) culture. Light microscope image, with a 400x magnification, of the primary LSEC culture the day after isolation. LSECs were isolated from mice's liver. Cells were maintained in complete William's E media with VEGF. The day after isolation, cells are ready for additional treatments.

To confirm cell identity and purity, we characterized cell population by performing a FACS analysis of LSEC the day after isolation. Cells were first gated according to side and forward scatter to exclude debris and doublets (Figure 10A and B). DAPI stain was used to infer on viability, as only dead cells incorporate and are stained with this dye. As shown in Figure 10C, the large majority of the cells excluded DAPI stain, showing that they were viable. We also stained cells with fluorophore-conjugated antibodies. We used anti-CD146, which stains all endothelial cells, anti-stab2, which stains specifically liver sinusoidal endothelial cells, and anti-F4/80, which stains Kupffer cells. As shown in Figure 10, 90.83% of the viable cells were endothelial (Figure 10D), 59.50% were LSEC (Figure 10E), and only 0.83% were Kupffer cells (Figure 10F). Notably, concerning CD146 expression (Figure 10D), the separation between positive and negative cells is very clear. In contrast, in the case of stab2, there was a continuum of expression levels, without a clear separation between positive and negative cells (Figure 10E). Similar patterns were observed when the results were plotted with F4/80 staining (Figure 10G and H).

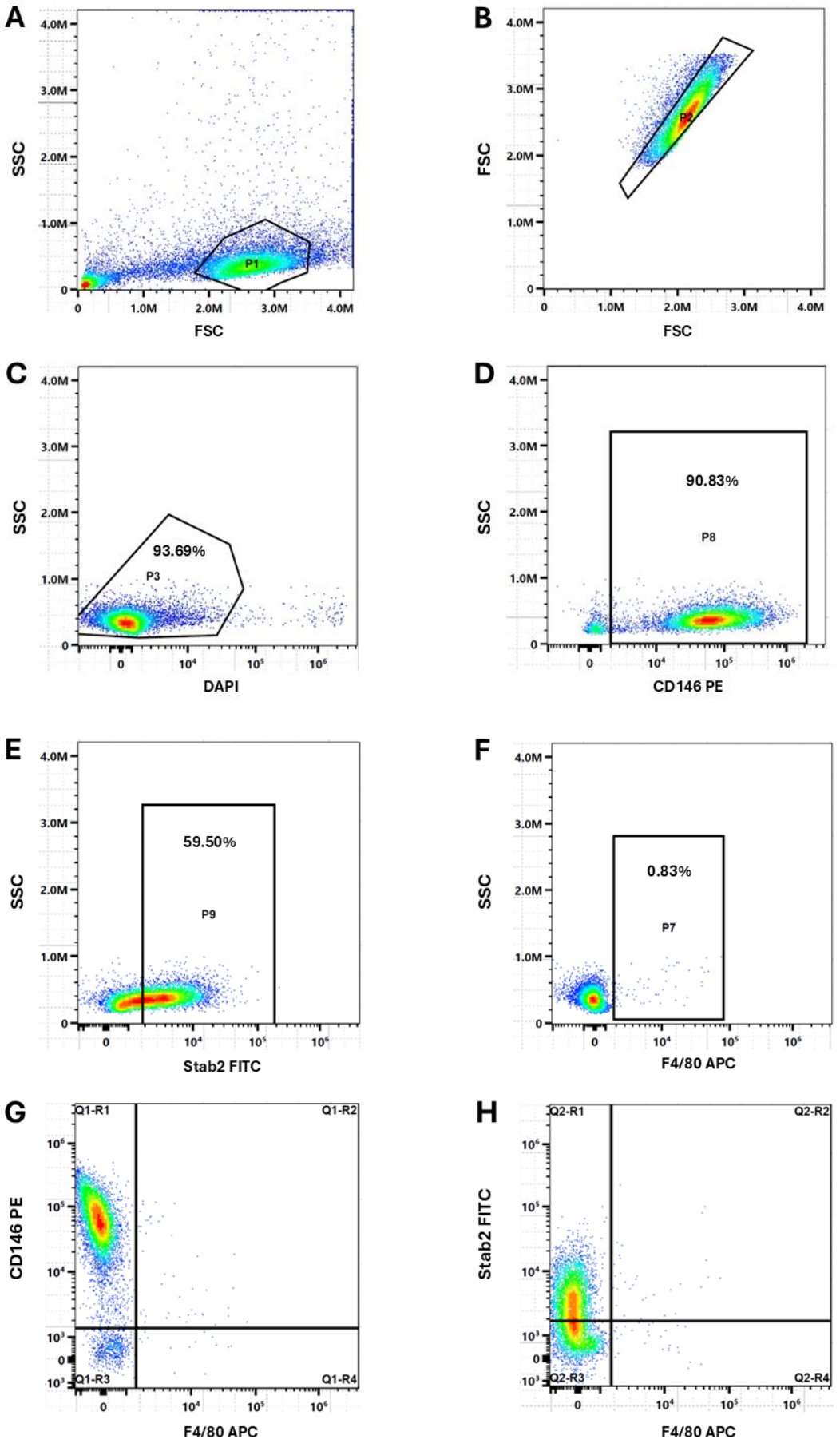

A
SSC
FSC
P1
B
FSC
FSC
P2
C
SSC
DAPI
93.69%
P3
D
SSC
CD146 PE
90.83%
P8
E
SSC
Stab2 FITC
59.50%
P9
F
SSC
F4/80 APC
0.83%
P7
G
CD146 PE
F4/80 APC
Q1-R1
Q1-R2
Q1-R3
Q1-R4
H
Stab2 FITC
F4/80 APC
Q2-R1
Q2-R2
Q2-R3
Q2-R4

Figure 10 - Fluorescence-Activated Cell Sorting (FACS) analysis of primary liver sinusoidal endothelial cells (LSECs) 1 day post-isolation. FACS plots showing the distribution of different markers expressed in LSECs the day after their isolation. LSECs were cultured, plated, and collected the following day as described in the Methods section for flow cytometry analysis. Cellular autofluorescence was measured and accounted for in all measurements. Cells were gated based on forward (FSC) and side scatter (SSC) (A and B) to exclude debris and doublets, as detailed in the Methods section. Cells were stained with DAPI (C), as well as with fluorophore-conjugated antibodies against CD146 (D and G), Satb2 (E and H), and F4/80 (F, G, and H). The percentage of positive (C, D, and E) or negative (F) populations is indicated in each quadrant. The plots show data from one independent experiment. Analysis performed in CYTEK AURORA.

2. Iron-related characterization under basal conditions

Once the primary cell cultures were established, we sought to characterize each cell type in terms of iron metabolism under basal conditions.

2.1 Iron-related gene expression

Firstly, we evaluated the expression of iron-related genes, alongside the expression of the housekeeping gene *Hprt1,* by qRT-PCR.

As shown in Figure 11, under basal conditions, BMM expressed both subunits of FT at high levels. These cells expressed *Bmp6*, *Fpn*, and *TfR1* at relatively lower levels.

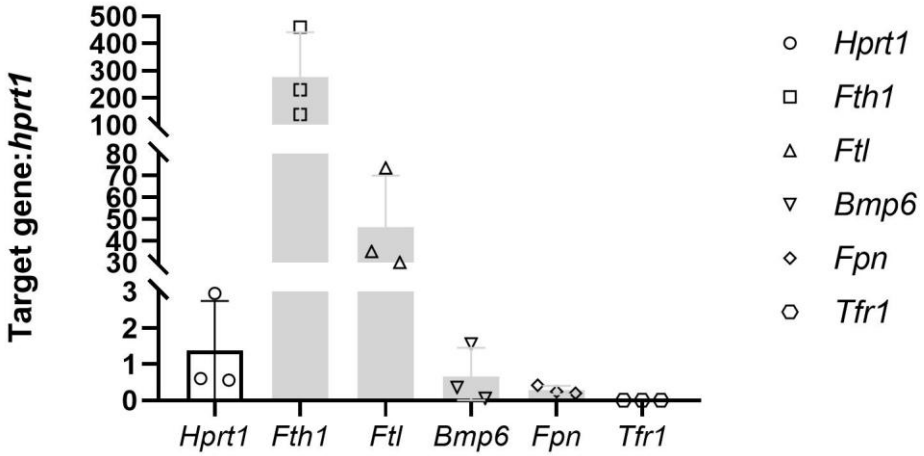


Figure 11 - qRT-PCR analysis of iron-related genes expression in BMM under basal conditions. The expression of *Fth1*, *Ftl*, *Bmp6*, *Fpn*, and *Tfr1* was quantified through qRT-PCR and normalized against the expression of *Hprt1*. Each bar corresponds to the mean + standard deviation of the values obtained in three independent experiments. Each symbol represents the mean of two technical replicates from the same experiment.

Regarding hepatocytes, the relative expression of the different iron-related genes was similar to those observed in BMM, with both subunits of FT showing higher expression levels than the other genes, under basal conditions (Figure 12). Interestingly, hepatocytes showed a relatively lower expression of *Bmp6* and higher expression of *Fpn*, compared with BMM (Figures 11, 12).

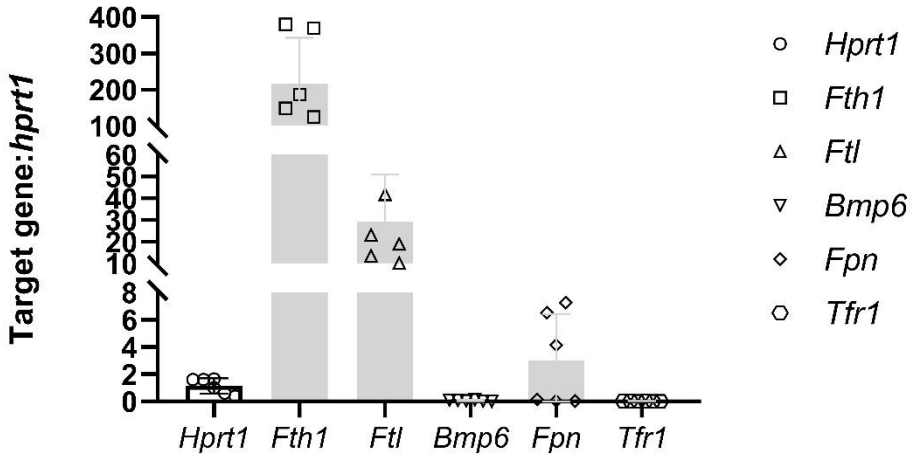


Figure 12 - qRT-PCR analysis of iron-related genes expression in hepatocytes under basal conditions. The expression of *Fth1*, *Ftl*, *Bmp6*, *Fpn*, and *Tfr1* was quantified through qRT-PCR and normalized against the expression of *Hprt1*. Each bar corresponds to the mean + standard deviation of the values obtained in three independent experiments. Each symbol represents the mean of two technical replicates from the same experiment.

In LSECs, only *Bmp6* expression was evaluated. This gene is characteristic of this cell type and is induced by iron and other stimuli. *Bmp6* expression was found in our LSEC, along with some variability across independent experiments (Figure 13).

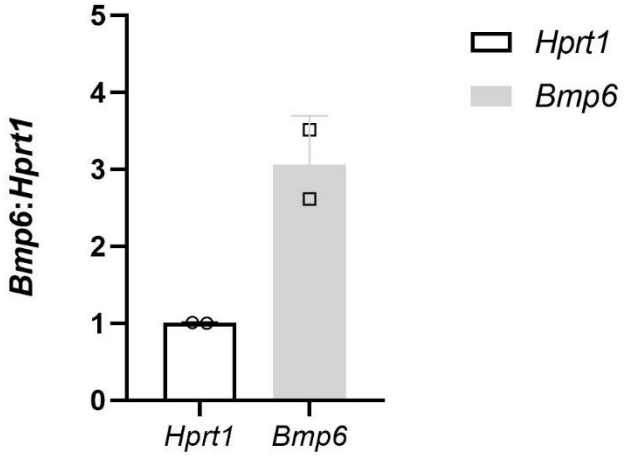


Figure 13 - qRT-PCR analysis of *Bmp6* expression in LSEC under basal conditions. The expression of *Bmp6* was quantified through qRT-PCR and normalized against the expression of *Hprt1*. Each bar corresponds to the mean + standard deviation of the values obtained in two independent experiments. Each symbol represents the mean of two (*Hprt1*) or three (*Bmp6*) technical replicates.

2.2 FT synthesis and release

Ferritin is one of the proteins that our group previously identified as key for iron-related intracellular communication in the context of infection and inflammation. To evaluate FT protein production and release under basal conditions, both FT subunits were quantified in cell lysates and supernatants by ELISA. Importantly, FTH and FTL were quantified in both complete DMEM and William's E media only. We found the quantity of FT in those media to be negligible.

Regarding macrophages, as shown in Table 3, there is, on average, 897 ng of FTH per mg of total protein and 1.0 ng of FTL per mg of total protein intracellularly. While extracellularly, there is, on average, 4.2 ng of FTH per mg of total protein and 0.7 ng of FTL per mg of total protein.

Concerning primary hepatocytes, there is, on average, more than 946 ng of FTH per mg of total protein and 1.8 ng of FTL per mg of total protein in the lysates. While in the supernatants there is, on average, 1.9 ng of FTH per mg of total protein and 0.7 ng of FTL per mg of total protein (Table 3). The actual concentration of FTH in hepatocyte lysates was not determined due to challenges inherent to the technique.

Intracellular ferritin in LSEC was not quantified due to time constraints. In their supernatants, there is, on average, 0.2 ng of FTH per mg of total protein and 1.1 ng of FTL per mg of total protein (Table 3).

Table 3 - FTs quantification on lysates and supernatants of BMM, hepatocytes, and LSEC under basal conditions. FTH and FTL quantification in cell lysates (intracellular) and supernatants (extracellular) of macrophages (BMM), hepatocytes (PH), and LSEC under basal conditions. Quantification was performed by ELISA. For the quantification in lysates, each value corresponds to the mean of two technical replicates. For the quantification in supernatants, each value corresponds to the mean of five (BMM), two (PH and FTH in LSEC) or four (FTL in LSEC) independent experiments.

		ng FTH/ mg Protein	ng FTL/ mg Protein
BMM	**Intracellular**	897	1.0
	Extracellular	4.2	0.7
PH	**Intracellular**	> 946	1.8
	Extracellular	1.9	0.7
LSEC	**Intracellular**	---	---
	Extracellular	0.2	1.1

Furthermore, we evaluated FT's presence in BMM and hepatocytes supernatants by western blot. As demonstrated in Figure 14, both FTH and FTL are present in the supernatants of macrophages and hepatocytes under basal conditions. Additionally, we assessed the presence of CD63 in BMM supernatants. CD63 is an EV marker reported to be present in EVs that carry iron-loaded ferritin [12]. We observed that CD63 is also present in the extracellular environment of BMM (Figure 14A).

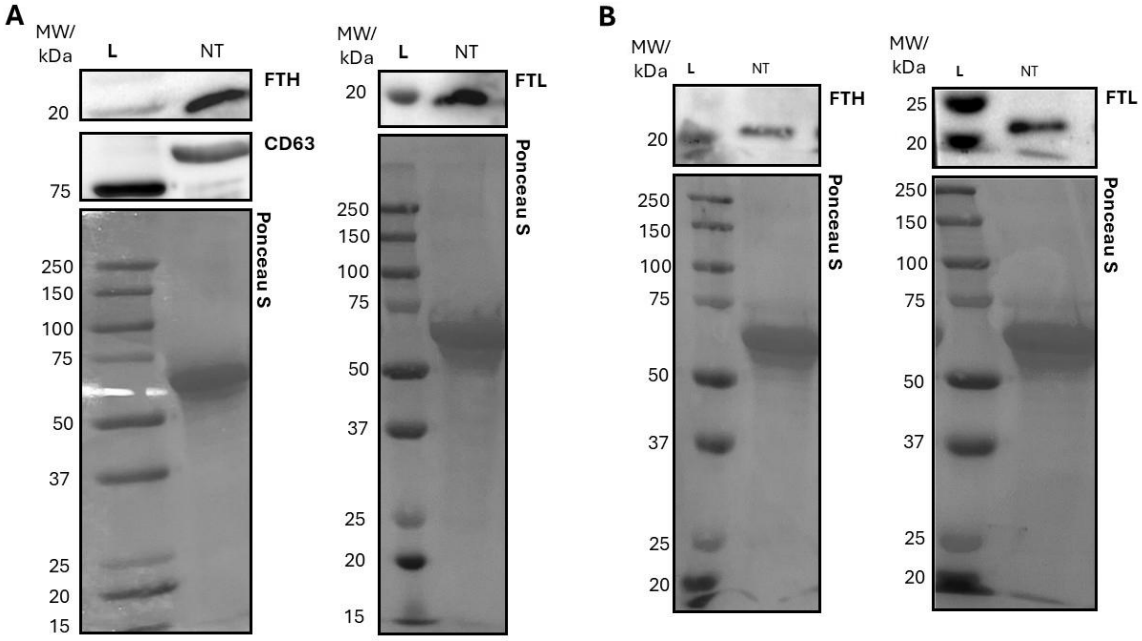


Figure 14 - Western blot of FTH, FTL and CD63 on BMM and hepatocytes supernatants. FTH, FTL, and CD63 presence in BMMs' concentrated supernatants was evaluated through Western blot (A). FTH and FTL presence in hepatocytes' concentrated supernatants was evaluated through Western blot (B). The membrane was stained with Ponceau S, and proteins of interest were marked using specific antibodies. Each membrane shows data from one independent experiment. The standards ladder (L) is presented in each membrane, and the molecular weight (MW) is displayed.

2.3 Intracellular iron quantification

Iron intracellular levels were quantified for all three types of cells.

As shown in Table 4, on average, BMM under basal conditions have 177.84 μg/L of intracellular iron. Hepatocytes have on average 105.39 μg/L of intracellular iron. In LSEC, the iron intracellular concentration has an average of 52.68 μg/L.

Table 4 - Intracellular iron content in BMM, hepatocytes (PH), and LSEC under basal conditions. Iron was quantified by atomic absorption spectrometry. Each value of iron concentration (μg/L) corresponds to the mean ± standard deviation of three (BMM) or two (PH) independent experiments. In the case of LSEC, only one independent experiment was performed and the value corresponds to the mean of technical replicates. For each sample, two technical replicates were performed.

	BMM	**PH**	**LSEC**
[Fe] (mg/L)	177.84 ± 70.87	105.39 ± 10.10	52.68

3. Iron-related characterization upon various stimuli

After establishing the iron-related characteristics of each cell type under basal conditions, we investigated how these characteristics were influenced by external stimuli. Specifically, we examined the effects of iron overload (FAC treatment), intracellular infection (with *M. avium*), and inflammatory activation (LPS, TNF-α, or FSL-1).

3.1 Iron-related gene expression

Firstly, we quantified the expression of iron-related genes in the three cell types by qRT-PCR. The relative expression of the target genes was normalized to *Hprt1* expression.

As shown in Figure 15, there are no significant differences in expression of the analysed genes when BMM were infected with *M. avium* for 48h.

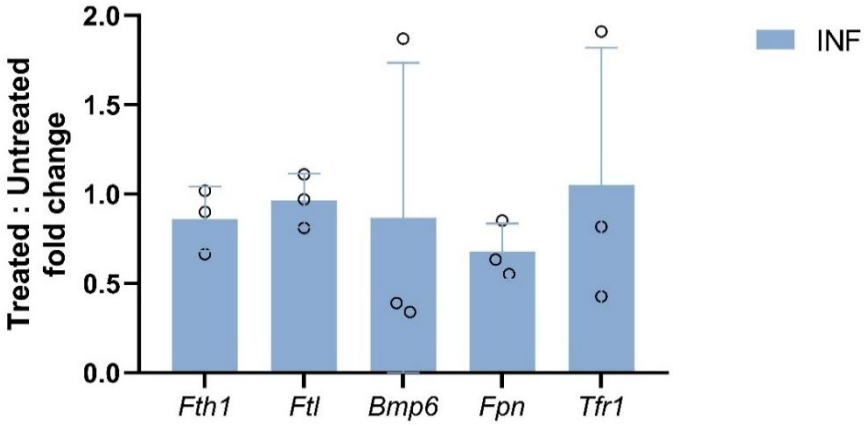


Figure 15 - qRT-PCR analysis of iron-related gene expression in infected BMM. BMM were infected with M. avium for 48h (INF). The expression of Fth1, Ftl, Bmp6, Fpn, and Tfr1 was quantified through qRT-PCR. The relative expression of each gene was normalized to the expression of Hprt1. Each bar corresponds to the mean + standard deviation of the fold change in gene expression relative to untreated samples, in three independent experiments. Each symbol represents the mean of two technical replicates from the same experiment. Statistics: t-test.

Regarding hepatocytes, as shown in Figure 16, iron overload did not significantly alter the expression of any of the genes tested. However, *Fth1* and *Ftl* showed a tendency to increase, whereas *Bmp6* and *Tfr1* tended to be expressed at lower levels when hepatocytes were treated with FAC. Additionally, LPS treatment did not noticeably affect the expression of any of the FT subunits genes, *Fpn* or *Bmp6*. In contrast, LPS increased *Tfr1* expression. These results should, however, be considered preliminary, as they are based on a single independent experiment.

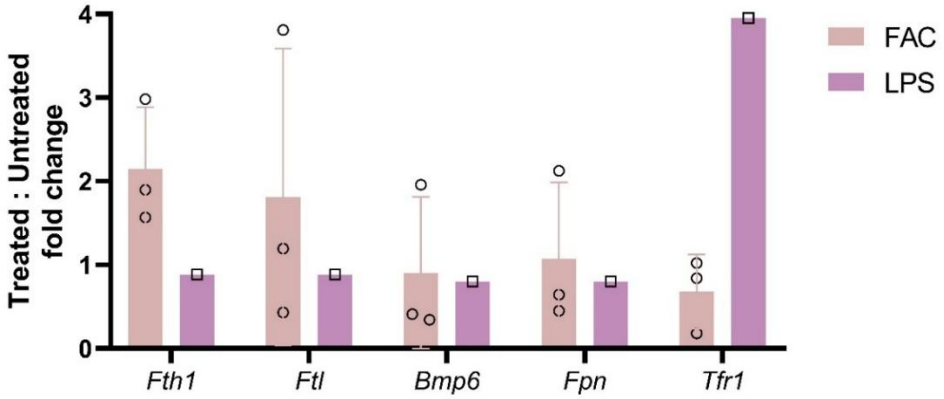


Figure 16 - qRT-PCR analysis of iron-related gene expression in hepatocytes following iron overload (FAC) or LPS treatment (LPS). Hepatocytes were treated with 100 μM FAC for 24h or with 10 ng/mL LPS for 48h. The expression of *Fth1*, *Ftl*, *Bmp6*, *Fpn*, and *Tfr1* was quantified through qRT-PCR. The relative expression of each gene was normalized to the expression of *Hprt1*. Each bar corresponds to the mean + standard deviation fold change (relative to untreated samples) of the values obtained in three (FAC) or one (LPS) independent experiments. Each symbol represents the mean of two technical replicates from the same experiment. Statistics: t-test.

Concerning LSEC, the impact of iron overload on *Bmp6* expression was evaluated. In this case, cells were incubated with either starvation or hepatocyte conditioned media and treated with FeNTA for 6h, and Bmp6 expression was quantified as described above.

As shown in Figure 17, when cells are incubated with starvation media, Bmp6 expression is not affected by iron overload. Nonetheless, when the incubation is performed with conditioned media, this is not the case. With hepatocyte media, in the absence of FeNTA, *Bmp6* expression has a small decrease, whereas in the presence of the iron source, *Bmp6* is slightly overexpressed.

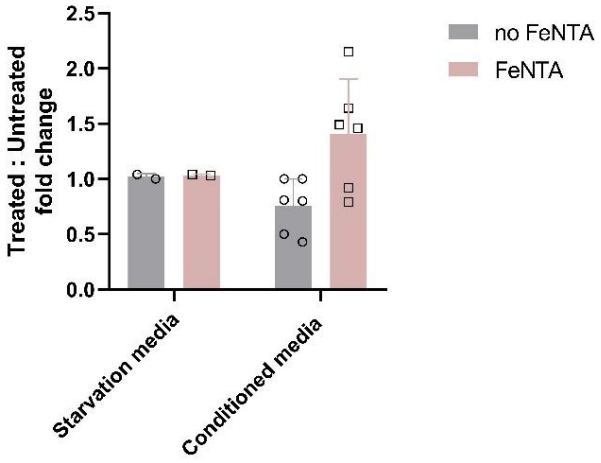


Figure 17 - qRT-PCR analysis of iron-related genes expression in LSEC. LSEC were either incubated in William's E medium with VEGF and no FBS (starvation media) or hepatocyte conditioned media for 1h. Cells were then treated with 0.25 μM FeNTA for 6h. The expression of *Bmp6* was quantified through qRT-PCR. The relative expression of each gene was normalized to the expression of *Hprt1*. Each bar corresponds to the mean + standard deviation fold change (relative to cells treated with starvation media only) of the values obtained from one (cells incubated with starvation media) or three independent experiments (cells incubated with conditioned media). Each symbol represents the mean of two technical replicates. Statistics: t-test.

3.2 FT synthesis and release

FT protein production and release were also assessed after cells were subjected to various stimuli.

We quantified both subunits of FT in BMM lysates. Of note, quantification was only performed for one independent experiment. Nonetheless, as demonstrated in Figure 18A, iron overload led to a slight decrease in intracellular FTL levels. When BMM were infected for 48h, neither FT subunits seemed to undergo a change in intracellular protein levels (Figure 18B).

Moreover, we evaluated the FT presence in macrophage supernatants. The supernatants were concentrated before quantification to allow protein detection. As demonstrated in Figure 18C, BMM subjected to iron overload had both subunits of FT, as well as CD63, in their supernatants. The qualitative analysis by Western blot indicated some variability between the two independent experiments. Moreover, CD63 and FTL presence in BMM supernatant did not seem to vary with iron overload. Nevertheless, a quantification was performed by ELISA. As shown in Figures 18D and E, neither the treatment with FAC nor the infection with *M. avium* led to a variation in neither FTH or FTL's presence in the supernatant of the cells.

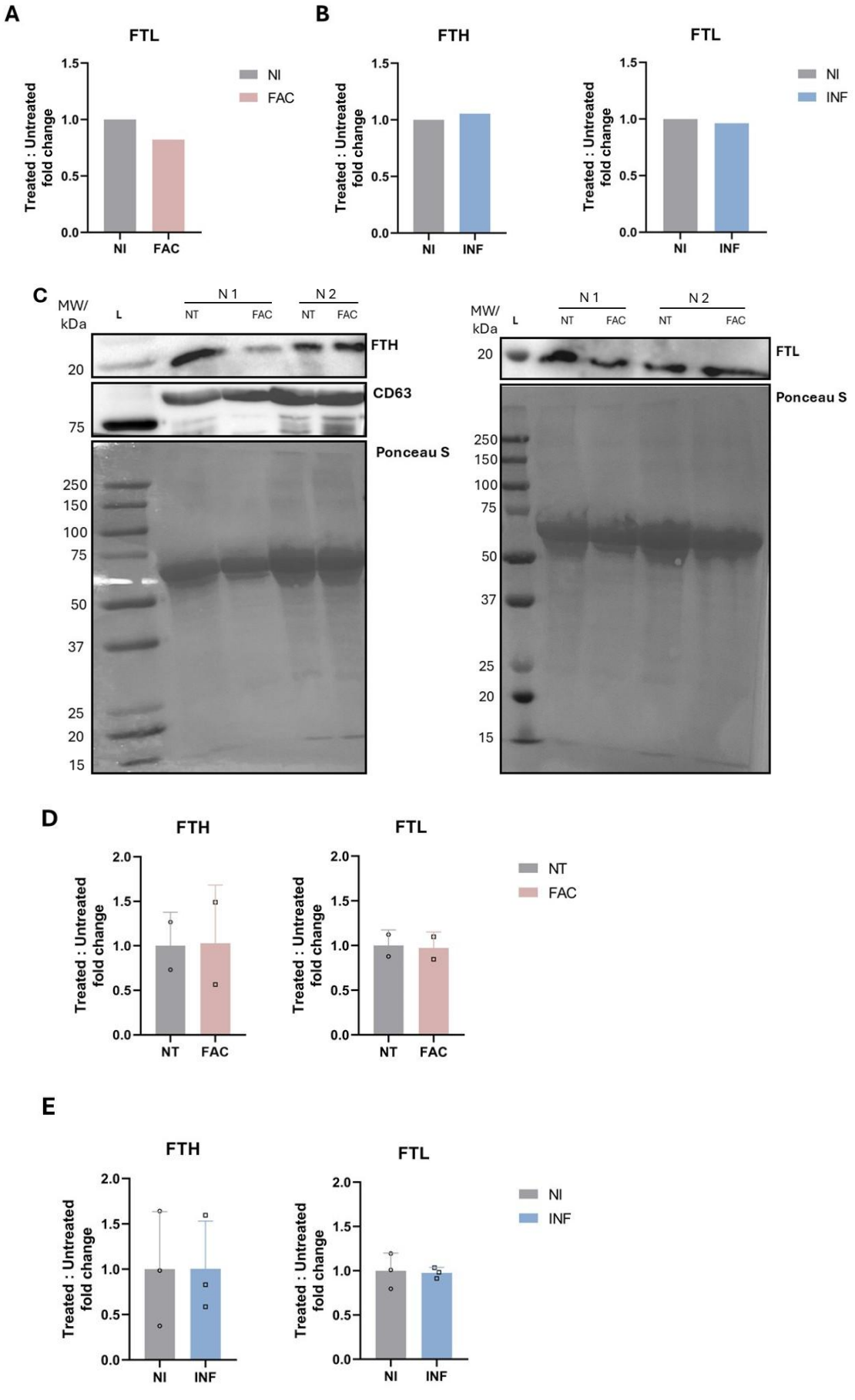

A
FTL
Treated : Untreated fold change
1.5
1.0
0.5
0.0
NI
FAC
B
FTH
FTL
NI
INF
C
MW/ kDa
L
N 1
N 2
NT
FAC
FTH
CD63
Ponceau S
20
75
250
150
100
50
37
25
15
D
FTH
FTL
2.0
NT
FAC
E
FTH
FTL

Figure 18 - FT quantification in BMM. FT in cell lysates and concentrated supernatants of non-treated (NT) macrophages, and macrophages treated with 10 μM FAC (FAC) or infected with *M. avium* (INF) for 48h were quantified. A. FTL in iron-loaded BMM lysates was quantified by ELISA. Each column represents the mean fold change (relative to untreated cells) of two technical replicates from one independent experiment. Statistics: t-test. B. FTH and FTL in infected BMM lysates were quantified by ELISA. Each column represents the mean fold change (relative to untreated cells) of two technical replicates from one independent experiment. Statistics: t-test. C. FTH, CD63, and FTL presence in concentrated supernatants was evaluated through Western blot. The membrane was stained with Ponceau S, and proteins of interest were marked using specific antibodies. Each membrane shows data from two independent experiments. The standards ladder (L) is represented in each membrane, and the molecular weight (MW) is displayed. N1 and N2 correspond to one independent experiment each. D. The total FT, FTH, and FTL in the supernatants of iron-loaded BMM was quantified by ELISA. Each bar corresponds to the mean + standard deviation fold change (relative to untreated cells) of the values obtained in two independent experiments. Each symbol represents the mean of two technical replicates from the same experiment. Statistics: t-test. E. The FTH, and FTL in supernatants of infected BMM was quantified by ELISA. Each bar corresponds to the mean + standard deviation fold change (relative to untreated cells) of the values obtained in two independent experiments. Each symbol represents the mean of two technical replicates from the same experiment. Statistics: t-test.

Additionally, we quantified FTL in hepatocyte lysates. As shown in Figure 19A, FTL is present at higher levels inside iron-overloaded cells, compared to non-treated ones. Moreover, we evaluated the presence of FT in cells' supernatants. These supernatants were also concentrated before quantification to allow protein detection. As shown in Figure 19B, both subunits of FT were present in these cell's supernatants. The qualitative analysis by western blot suggested that there was only a significant increase in the amount of FTH in supernatants, upon iron overload, in one of the independent experiments. Besides a qualitative analysis, a quantification was performed by ELISA. As shown in Figure 19C, there was a tendency for an increase in extracellular FTH upon iron overload. Regarding the L subunit, iron treatment did not seem to have any impact.

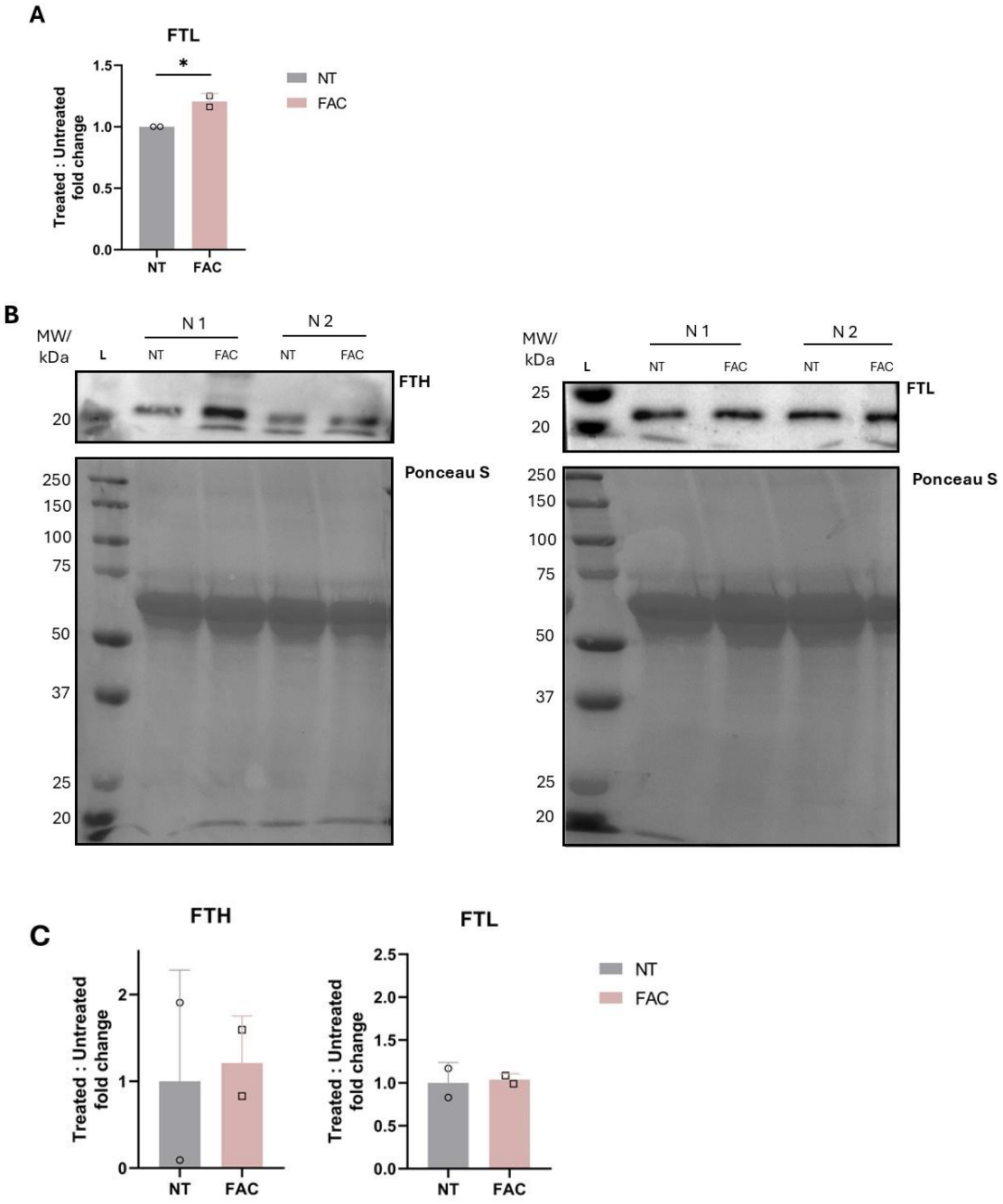


Figure 19 - FT quantification in hepatocytes. FT in cell lysates and concentrated supernatants of non-treated hepatocytes (NT) and hepatocytes treated with 100 μM FAC for 24h (FAC) were quantified. A. FTL in hepatocyte lysates was quantified by ELISA. Each bar corresponds to the mean + standard deviation fold change (relative to untreated cells) of the values obtained in two independent experiments. Each symbol represents the mean of two technical replicates from the same experiment. Statistics: t-test. *p<0.05. B. FTH and FTL presence in concentrated supernatants was evaluated through Western blot. The membrane was stained with Ponceau S, and FTs were marked using specific antibodies. Each membrane shows data from two independent experiments. The standards ladder (L) is represented in each membrane, and the molecular weight (MW) is displayed. N1 and N2 correspond to one independent experiment each. C. The FTH, and FTL in concentrated supernatants was quantified by ELISA. Each bar corresponds to the mean + standard deviation fold change (relative to untreated cells) of the values obtained in two independent experiments. Each symbol represents the mean of two technical replicates from the same experiment. Statistics: t-test.

Regarding LSECs, only data on FT presence in supernatants were collected. Both subunits were quantified in LSEC supernatants by ELISA. As shown in Figure 20, none of the inflammatory stimuli strongly impacted FTH and FTL presence in the extracellular environment. Despite that, there seem to be different tendencies comparing the treatments. TNF-α induces a slight increase in FTH levels in the supernatant, whereas FSL-1 appears to reduce them. In contrast, TNF-α has virtually no effect on FTL, while FSL-1 leads to a modest increase in its levels in the supernatant.

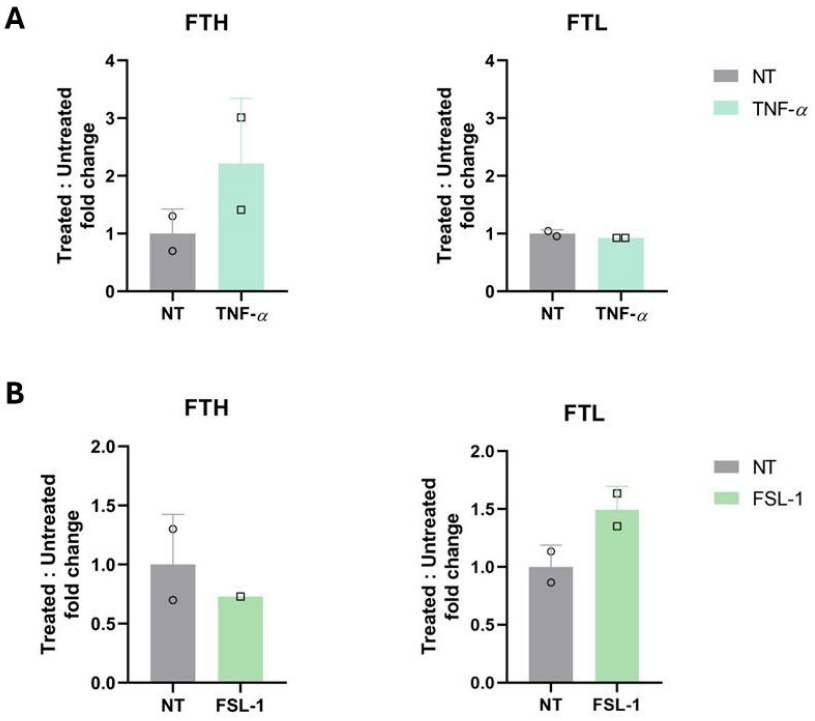


Figure 20 - FT quantification on LSEC supernatant upon inflammatory stimuli. LSEC were untreated (NT) or incubated with 10 ng/mL of TNF-α or 100 ng/mL of FSL-1 for 24h. FTH and FTL in LSEC supernatants were quantified through an ELISA. Each bar corresponds to the mean + standard deviation fold change (relative to untreated cells) of the values obtained in two independent experiments. Each symbol represents the mean of two technical replicates from the same experiment. Statistics: t-test.

3.3 Intracellular iron quantification

Intracellular iron was measured for BMM subjected to iron overload and *M. avium* infection. This was also performed for LSEC stimulated with TNF-α and FSL-1.

As shown in Figure 21A, incubation with FAC actually translates into an increase of this element inside macrophages, although only one independent experiment was performed. In contrast, infection leads to a small decrease in iron content in BMM (Figure 21B).

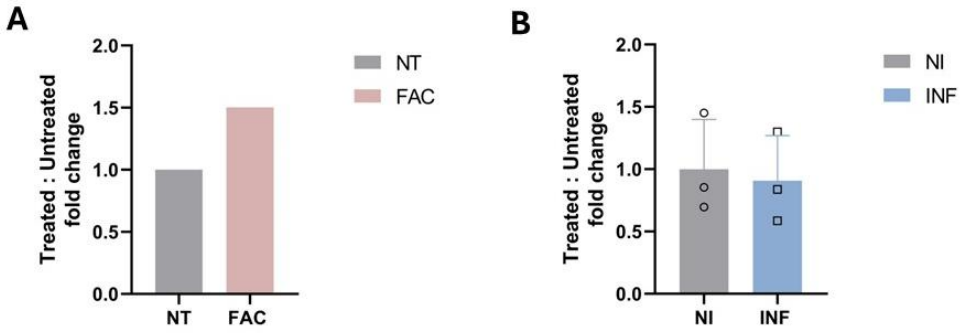


Figure 21 - Iron intracellular quantification in stimulated BMM. A. Intracellular iron quantification in BMM upon iron overload. BMM were treated with 10 μM FAC for 48h. Each column represents the mean fold change (relative to untreated cells) of two technical replicates from one independent experiment. B. Intracellular iron quantification in BMM upon a 48h *M. avium* infection. Each bar corresponds to the mean + standard deviation fold change (relative to untreated cells) of the values obtained in three independent experiments. Each symbol represents the mean of two technical replicates from the same experiment.

Regarding LSEC, as shown in Figure 22, inflammation seemed to lead to a slight decrease in intracellular iron, although more experiments need to be performed.

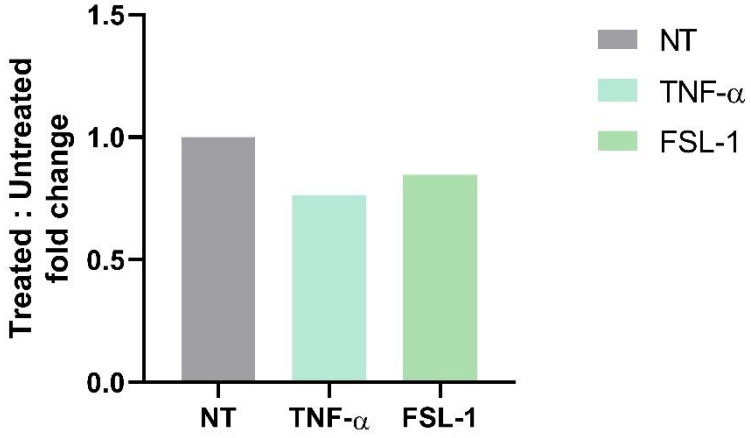


Figure 22 - Iron intracellular quantification in stimulated LSEC. LSEC were treated with 10 ng/mL of TNF-α or 100 ng/mL of FSL-1 for 24h. Each column represents the mean fold change (relative to untreated cells) of two technical replicates from one independent experiment.

4. Iron-related gene expression in hepatocytes upon intercellular communication

At last, we aimed to investigate the iron-related intercellular communication between BMM or LSEC and hepatocytes, namely upon infection and inflammation.

We assessed the effects of inflammatory stimuli on LSEC-Hepatocyte communication. The goal was to determine how paracrine signalling from stimulated LSECs affects hepatocyte iron metabolism. Thus, we treated LSEC with TNF-α and FSL-1 and collected their conditioned media (L-CM). Then, we treated hepatocytes with that medium and quantified iron-related gene expression in hepatocytes. As controls, we incubated hepatocytes with their normal media, complete William's E, and with their normal media supplemented with VEGF. This second control group was added once LSEC conditioned media contained VEGF, otherwise, cells would start to transdifferentiate.

Iron-related genes were evaluated, and their relative expression was normalized to *Hprt1* expression. Additionally, to allow comparison across conditions, each gene's expression was further normalized to its level in untreated samples (Figure 23A).

As shown in Figure 23A, *Fth1* expression slightly decreases when the media contains VEGF. When hepatocytes are treated with LSEC conditioned media with no stimuli, they remain practically the same in relation to cells incubated with normal media. However, TNF-α and FSL-1 stimulation of LSEC leads to an increase in *Fth* expression, with the increase in the case of FSL-1 being significant.

Concerning *Ftl* expression, there is also a small decrease when the cell medium contains VEGF. In contrast with what happens for *Fth*, *Ftl* seems to be slightly under expressed when L-CM comes from non-treated cells or cells treated with TNF-α. On the other hand, when LSECs are stimulated with FSL-1, their conditioned media leads to a significant decrease in *Ftl* expression, compared to non-treated hepatocytes.

In relation to *Bmp6*, its expression is diminished when hepatocytes are treated with normal media with VEGF, and L-CM from non-treated cells or cells treated with FSL-1. This gene expression also decreases when hepatocytes are treated with L-CM from cells stimulated with TNF-α. Interestingly, among cells treated with the different L-CM, there are no differences concerning Bmp6 expression.

Regarding *Fpn*, VEGF has a significant negative impact on its expression. Despite leading to a decrease in expression, none of the L-CM seemed to produce such a difference in *Fpn* expression, compared to non-treated cells. However, *Fpn* expression is higher in hepatocytes treated with L-CM compared to hepatocytes that were in contact with normal media with VEGF. Notably, in the case of LSEC non-treated or treated with TNF-α, this difference is statistically significant.

Finally, *Tfr1* expression seems to remain unaltered by the treatments.

Furthermore, we studied the effects of indirect contact of hepatocytes and non-infected and infected BMM (BMM INF) on the expression of iron-related genes by the hepatic cells. Therefore, we co-cultured BMM with hepatocytes, with BMM being plated in trans-well inserts, and iron-related genes in hepatocytes were evaluated, and their relative expression was normalized to *Hprt1* expression (Figure 23B). Additionally, to allow comparison across conditions, each gene's expression was further normalized to its level in untreated samples.

Fth seems to be slightly underexpressed in hepatocytes when BMM are infected. *Ftl* and *Bmp6* expression remains virtually unchanged with infection. Regarding *Fpn*, independent experiments do not seem concordant. However, based on these data, Fpn expression does not appear to be affected by infection. In contrast, *Tfr1* is augmented in hepatocytes that come into contact with infected BMM.

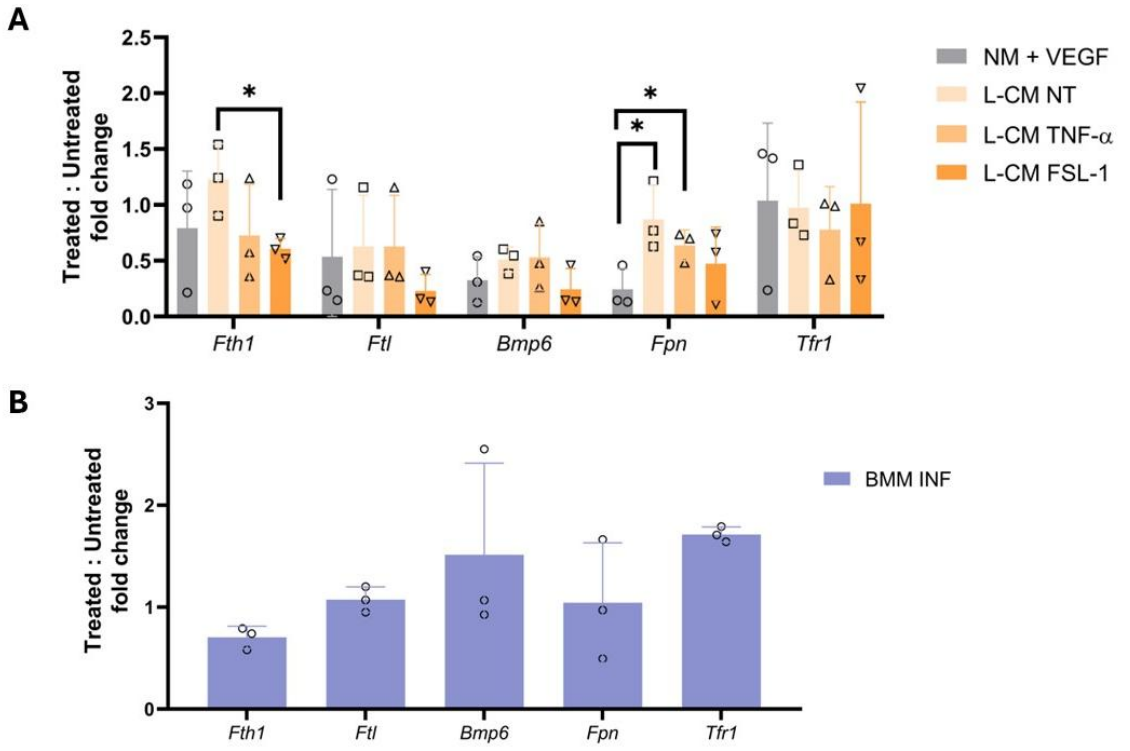


Figure 23 - qRT-PCR analysis of iron-related gene expression in hepatocytes following co-culture or conditioned media treatment. A. Hepatocytes were treated with complete William's E media (NM), complete William's E media with VEGF (NM + VEGF) or LSEC conditioned media (L-CM) for 6h. The L-CM was collected from untreated cells (L-CM NT) and cells that were treated with TNF-α (L-CM TNF-α) or FSL-1 (L-CM FSL-1). B. Hepatocytes were co-cultured with non-infected (NI) or infected BMM, with *M. avium*, (BMM INF) for 60h. The expression of *Fth1*, *Ftl*, *Bmp6*, *Fpn*, and *Tfr1* was quantified through qRT-PCR. The relative expression of each gene was normalized to the expression of *Hprt1*. Each bar corresponds to the mean ± standard deviation fold change (relative to untreated samples) of the values obtained in two (A) or three (B) independent experiments. Each symbol represents the mean of two technical replicates from the same experiment. Statistics: t-test. *p<0.05.

Discussion

The present project aimed to characterize the iron-related intercellular communication between different liver cell types, with a particular focus on inflammatory and infectious contexts. Although it is well established that such conditions alter iron homeostasis, how liver cells interact and coordinate their responses to said changes remains poorly understood.

We decided to focus on macrophages, hepatocytes, and LSEC. These cells, along with the communication between them, are central to both iron metabolism and response to infection and inflammation. Macrophages are key for iron homeostasis [4], the host cell of our model bacteria, *M. avium* [83], and play a pivotal role in modulating immune responses [71]. Hepatocytes are essential for maintaining systemic iron levels [3] and also contribute actively to the immune response [45]. LSECs, in turn, are involved in iron sensing and signaling [53, 54] while simultaneously participating in immune regulation [52].

The first step of this project was the establishment and optimization of primary cultures of the selected cell types.

As previously mentioned, to obtain macrophages, we used a very well-established protocol in Gomes' lab. In this protocol, we isolated macrophage progenitor cells from the bone marrow of mice and cultured these cells with a medium that contains M-CSF. This growth factor allows the differentiation of the progenitor cells into macrophages. As shown in Figure 6, cells transitioned from a small, round morphology to an elongated shape, consistent with that observed in fully differentiated macrophages. Importantly, the visual evaluation of the cells under an optical microscope indicated that the macrophages used in this project were similar to those that have been used in the group.

Furthermore, we are confident in declaring that this macrophage culture protocol allows us to obtain quality cells, as viability assays and population identification by flow cytometry have been performed and showed satisfying results [89].

For hepatocytes, we used a method published by Charni-Natan and colleagues with a few optimizations [97]. As hepatocytes are by far the most abundant cell type in the liver, their isolation from the organ, once it is digested, is somewhat trivial. Optical microscopy observations (Figure 7) allowed us to conclude that practically all the cells that adhered to the collagen-coated plate had the characteristic morphology of hepatocytes. Meaning the cells were large, cuboidal, and presented multiple nuclei. Nonetheless, we observed some cells in suspension that were either dead or another type of cell that does not

adhere to collagen. These cells were washed before further experiments were performed.

In order to have more robust data on this primary hepatocyte culture, we could have performed flow cytometry to determine the percentage of cells that displayed hepatocyte-specific markers.

Still regarding primary hepatocyte culture, these cells were intended to be used for iron overload experiments. As this was the first time such experiments were conducted in primary hepatocytes in Gomes' laboratory, establishing suitable conditions was important. Thus, hepatocytes were treated with various concentrations of FAC, and viability was assessed using a resazurin assay. We observed that hepatocyte viability was not impaired by FAC, even at 100 μM (Figure 8). Given the objective of inducing substantial iron overload, 100 μM FAC was selected for subsequent experiments.

Concerning LSEC, to obtain a primary cell culture, we applied a protocol established in Muckenthaler's laboratory, in which these endothelial cells are isolated from digested liver tissue using differential gradient centrifugations. The protocol is technically challenging as LSEC are not very abundant in the liver and are considerably attached to hepatocytes [51]. Moreover, the cells are highly susceptible to stress, which leads to their death or trans differentiation [101]. Regarding the procedure, during the initial centrifugations, non-parenchymal cells (LSECs, HSCs, and KCs) are separated from hepatocytes. If the organ digestion is not thorough, LSEC will still be attached to hepatocytes, significantly reducing the isolation yield. The centrifugation with the gradient aims to separate LSEC and KC from HSC, which are less dense. If this step is not well performed, the final LSEC population will be contaminated with HSC. Finally, LSECs are distinguished from KCs based on their inability to adhere to plastic surfaces. After incubation in six-well plates, LSECs remain in suspension, while KCs attach. Nevertheless, even with careful washing to recover LSECs, some degree of KC contamination may still occur.

Despite the technical challenges associated with LSEC isolation, we successfully cultured primary LSEC. Optical microscopy observations showed that the cells in culture were small and roundish and had elongated extremities, compatible with the typical LSEC morphology (Figure 9).

With the purpose of confirming that the cultured cells were LSEC, we performed FACS analysis one day after isolation. Importantly, the analysis demonstrated that the vast majority of cells were viable (Figure 10C).

Moreover, almost all cells were positive for CD146, an endothelial marker (Figure 10D). Since nearly all endothelial cells in the liver are LSEC [48], the predominance of CD146-positive cells in our sample strongly supports that the cultured population consists primarily of LSEC.

Regarding staining with stab2, a specific marker of LSEC, there is no clear distinction between unstained and stained cells. Of note, approximately 60% of the analyzed cells could be confidently identified as LSEC. The lack of clear separation between positive and negative cells could either be explained by the low binding capacity of the antibody or by the trans differentiation of the cells.

In order to further confirm the cell's identity and differentiation state, we could use scanning electron microscopy to visualize the *fenestrae*. The presence of these LSEC-specific structures would confirm the identity and quality of the cells [51, 102]. Due to time constraints, we were unable to perform this experiment. Nevertheless, the high percentage of endothelial cells observed provided sufficient confidence to proceed with further experiments.

Moreover, the very low percentage of F4/80 (macrophage-specific marker)-positive cells indicates that the contamination by KC is minimal.

With the primary cell cultures successfully established, we proceeded to characterize their iron metabolism under basal conditions, as a foundation for subsequent experiments.

Firstly, we assessed the expression of several iron-related genes in the three cell types.

As shown in Figures 11 and 12, BMM and hepatocytes showed a similar pattern when it comes to the relative expression of the iron-related genes analyzed. Under basal conditions, these cells expressed both subunits of FT at significantly higher levels compared to the reference gene. This is probably because macrophages and hepatocytes are the main iron storage cells in the organism. Thus, they need the iron storage protein in high quantities even when unstimulated. Conversely, *Bmp6 was* expressed at lower levels compared to *Hprt1*. *Fpn* is also expressed at lower levels in both cell types, probably because, under basal conditions, they do not need to export iron. Tfr1 was expressed at very low levels as well. The cause of this observation might be that the cells are not iron-deficient, so they do not need to express a protein responsible for iron uptake. Additionally, in the case of macrophages, there are other mechanisms to acquire iron, such as the phagocytosis of senescent red blood cells.

Of note, caution should be applied to the interpretation of the data corresponding to the expression of *Fpn* in hepatocytes, which seems to have a bimodal distribution, with higher levels in 3 experiments and lower levels in the other 3 experiments. These correspond to experiments performed either in Gomes or in Muckenthaler's laboratories. Data obtained from hepatocytes cultured in Gomes' lab indicates *Fpn* is less expressed, whereas data from cells isolated in Muckenthaler's lab show this gene is more expressed. Of note, the method for the isolation of the hepatic cells in both laboratories was also different. However, culture maintenance followed the same procedures, and the same medium is used. (Figure 12). Further studies would be needed to clarify this issue.

For LSEC, we only evaluated *Bmp6* expression (Figure 13). LSEC lysates for the evaluation of the other genes were collected in Muckenthaler's lab and shipped to i3S for further processing and gene expression evaluation. However, when RNA quality was assessed, we discovered it was not satisfactory and decided not to continue with the analyses.

Regarding *Bmp6* expression, although there is a substantial variability observed across independent experiments, we observed a tendency for an elevated expression relative to the housekeeping gene. This is because there is always a basal expression of *Bmp6*, even when iron levels are not elevated [23]. The heterogeneity seen among independent experiments might be due to the inherent variability of primary cell cultures. However, other factors can be interfering with *Bmp6* expression in LSEC, as this gene is induced in stress conditions [103].

Moreover, we quantified the two ferritin subunits in both cell lysates and supernatants.

As shown in Table 3, there were considerable amounts of FTH and FTL in the lysates of macrophages and hepatocytes, although FTL concentration was lower. This is concordant with the high levels of the mRNA of both subunits in both cell types (Figures 11 and 12). The results were expected as macrophages and hepatocytes are the main cell types responsible for intracellular iron storage, needing ferritin to perform that role properly.

Of note, the amount of FTL was much lower than the amount of FTH. This observation contrasts with what has been reported in the literature for hepatocytes [104]. In the case of macrophages, there is evidence that suggests that, in fact, there is more FTH than FTL in these cells [105].

Regarding extracellular ferritin, as shown in Figure 14, both subunits are detected by western blot in macrophage and hepatocyte supernatants. We attempted to quantify the bands, however, once the bands' areas are used in the calculation and the bands had substantial different areas, it was not possible to obtain reliable results.

Thus, we quantified FTH and FTL in the cells' supernatants by ELISA (Table 3). As mentioned previously, we assessed the concentration of both subunits of FT in complete DMEM and William's E media alone and found the concentrations to be negligible. Thus, once we were able to quantify higher levels of FTH and FTL in the supernatants of all the cell types, we concluded that macrophages, hepatocytes, and LSEC are able to release both subunits of FT.

Notably, it has been previously demonstrated that macrophages and hepatocytes may be able to release FT [106, 107]. In contrast, it has not been reported that LSEC release this protein.

Interestingly, we observed that, despite hepatocytes containing more FTH intracellularly, the amount of the protein present in macrophages' supernatant is higher. This suggests that macrophages release more FTH than hepatocytes. Of note, while in the supernatants of hepatocytes and BMMs the amount of FTH is higher than that of FTL, the opposite is found in the case of LSEC. This suggests that the mechanisms of regulation of FT release may be different depending on the cell type.

Additionally, the presence of CD63 in BMM supernatants was also evaluated. As mentioned above, CD63 is an EV marker present in ferritin-loaded vesicles that fibroblasts release upon iron overload [12]. Our results confirmed that CD63 was also present in macrophages' supernatants. However, in the present work, we did not investigate whether this CD63 was associated with EVs.

Additionally, we quantified iron intracellular levels in the three cell types (Table 4). We observed that macrophages and hepatocytes contain more intracellular iron than LSEC, which is consistent with the fact that the first two cell types are the main responsible for iron storage.

With the behavior of the cells characterized under basal conditions, we aimed to investigate how different stimuli, namely iron overload, inflammation, and infection with *M. avium* would affect said behavior.

We started by evaluating iron-related gene expression in infected BMM (Figure 15). In contrast with what we expected [90]*, M. avium* did not impact the expression of the genes

analyzed. We speculate that the reason why the infection did not lead to a difference in gene expression is that its duration is not long enough. We observed that the CFU count only starts to increase at 5 days post-infection (data not shown). At 48h, the infection still has a limited impact on iron-related genetic expression. Thus, it would be important to repeat these experiments with a longer infection period.

Concerning hepatocytes, we evaluated the effects of both iron overload, induced by FAC treatment, and inflammation, triggered by LPS exposure (Figure 16).

As expected, iron overload results in an increased expression of *Fth1*. In contrast, the relative expression of *Ftl* under the same conditions is not consistent across the three independent experiments. Therefore, repeating this analysis with a larger number of samples could be valuable. Based on the current data, we observe a clear trend toward increased *Fth1* expression, but not *Ftl*. This discrepancy might reflect the higher demand for FTH subunit synthesis under iron overload, given the fact that this is the subunit responsible for the elements' incorporation into the ferritin nanocage [18].

Bmp6, *Fpn*, and *Tfr1* did not seem to have their gene expression altered upon FAC treatment. Since hepatocytes are the primary site of iron storage, even under iron overload conditions, *Fpn* expression could remain unchanged, as the metal remains within these cells for storage. However, in this case, *Fpn* could be regulated by the IRE-IRP system, explaining why no changes in mRNA levels are detected. *Tfr1* is expected not to be upregulated when intracellular iron levels increase, since its expression would promote further iron uptake.

LPS, a well-characterized component of the Gram-negative bacterial cell wall, is widely recognized for its ability to activate immune responses [27]. The effect of bacterial products in hepatocytes has been less explored. However, a recent publication showed that TLR activation in hepatocytes has an impact in iron-related gene regulation. For this reason, we used LPS to investigate the iron-related inflammatory response in hepatocytes [108].

Concerning our very preliminary data obtained from LPS-treated hepatocytes, inflammation did not seem to alter considerably the expression of *Fth1*, *Ftl*, *Bmp6*, or *Fpn*. Nonetheless, more experiments need to be performed to clarify this observation, as there seems to be a slight tendency for a downregulation of these genes upon stimulation with LPS.

In the case of the FT subunits, we were expecting an upregulation upon inflammatory stimuli, as that has been reported by different studies [107, 109]. In contrast, *Fpn* would

be expected to be downregulated in inflammatory conditions, in concordance with what has been reported [74, 110]. Nonetheless, we cannot disregard the post-transcriptional regulation by the IRE-IRP system that may be playing a role in these cases.

In contrast, *Tfr1* seemed to be upregulated in inflammatory conditions. Again, more experiments are needed to confirm the preliminary data. Nevertheless, we could speculate that hepatocytes under an inflammatory stimuli become more prone to incorporate and store iron. This is consistent with the idea that inflammation leads to a decrease in iron circulating levels and its intracellular accumulation.

Furthermore, *Tfr1* is upregulated when cells are iron-deficient, so this reason cannot be disregarded, and iron intracellular levels should be quantified.

Regarding LSEC, we evaluated the effects of paracrine communication with hepatocytes together with elevated iron levels (Figure 17). For this, cells were incubated either with William's media with no FBS or hepatocyte conditioned media, as well as FeNTA as an iron source. As reported by Colucci and colleagues, for LSEC to induce *Bmp6* expression, two conditions need to be met. The first one is increased iron levels, and the second one is the presence of a protein factor derived from hepatocytes. Our results are in concordance with this observation. Of note, the fact that *Bmp6* expression decreases in the mentioned condition has been observed in Muckenthaler's lab. We could speculate that hepatocyte conditioned medium also contains some kind of factor that inhibits *Bmp6* expression in the absence of increased iron levels.

Samples from LSEC stimulated with TNF-α and FSL-1 were generated in Muckenthaler´s lab and shipped to i3S for further processing and gene expression evaluation. However, when RNA quality was assessed, we discovered it was not satisfactory and decided not to continue with the analyses.

After completing the analysis of gene expression, we focused on the evaluation of FT at the protein level under the various stimuli.

We quantified FT in the lysates of BMM treated with FAC or infected with *M. avium* (Figure 18A and B). Of note, samples from only one independent experiment were analyzed and, in consequence, the results are very preliminary.

Upon iron overload, FTL seemed to be slightly less present in macrophages. FTH was also quantified, but concentration values could not be obtained by ELISA as the samples contains too much of this FT subunit.

Upon infection, a very slight increase in FTH and a very slight decrease in FTL were observed. We expected to verify a more prominent increase in the synthesis of both FT subunits. Yet, in parallel to what was seen at a gene level, there are no significant changes in FT production. We hypothesize that this is also linked to the short duration of the infection.

Intending to verify if macrophages' release of FT changes upon stimulation, we analyzed their supernatants.

The qualitative analysis of the western blot showed heterogeneous results, with iron overload leading to a decrease in one experiment and to an increase in the other. This was observed for both subunits. Regarding CD63, there seemed to be a slight increase in its presence in BMM supernatant upon iron overload (Figure 18C).

As mentioned above, we tried to perform a quantification of the western blot bands, but did not obtain reliable results.

Thus, FTH and FTL in BMM supernatants were quantified by ELISA (Figure 18D and E). In the case of BMM treated with FAC, there was no significant difference in the presence of either FT subunits in the supernatant. This was also observed for macrophages infected with *M. avium*.

The lack of differences registered contrasted with our expectations. It seems logical that upon iron overload, more FT would be released by macrophages, as shown in other cell types such as fibroblasts [12]. Moreover, it has been reported that macrophages release FTH when infected with *M. avium* [91], and during sepsis [11].

We hypothesized that neither the FAC treatment nor the infection was long enough to impact protein synthesis and release. Therefore, we propose to repeat the experiments with longer treatment periods.

Concerning hepatocytes, FTL was significantly more present in these cells upon iron overload (Figure 19A). Of note, *Ftl* expression was not upregulated in hepatocytes in these conditions (Figure 16). This suggests that FTL synthesis is being promoted by the IRE-IRP system, which regulates iron-related protein expression at a post-transcriptional level.

FTH was also quantified, however, as previously explained, there was too much of this subunit in both untreated and treated samples to obtain values by ELISA. Therefore, we can only conclude that in both cases, hepatocytes synthesize large amounts of FTH.

Then, with the goal of verifying if hepatocytes' release of FT changes upon stimulation, we analyzed their supernatants.

The qualitative analyses of the western blot showed high variability among independent experiments when it comes to FTH release. In only one of the experiments, the increased release seemed to be significant. Regarding FTL, iron overload in hepatocytes did not seem to lead to a difference in its release (Figure 19B).

FTH and FTL in hepatocytes' supernatants were quantified by ELISA (Figure 19C). The observations made with western blot seem to be corroborated by the quantification by ELISA. FTH results are variable, but there was a tendency for an increase in release upon iron overload. While FTL release seemed to be unaltered by the FAC treatment. Once again, we were expecting a clearer increase in FT release upon iron overload.

Concerning LSEC, only quantification of FTH and FTL in the supernatants was performed by ELISA (Figure 20). The quantification was performed in non-treated LSEC and LSEC stimulated with pro-inflammatory factors, TNF-α and FSL-1. TNF-α is the pro-inflammatory cytokine that macrophages release upon infection with *M.avium*. FSL-1 is a lipoprotein ligand from *Mycoplasma salivarium* known to activate TLR2 [74], the same TLR that *M. avium* activates [90]. Thus, these factors were selected as they might provide insight into the potential results of an M. avium infection on LSEC iron-related metabolism.

TNF-α led to a slightly increased release of FTH by LSEC. FSL-1 seemed to lead to a modest decrease in FTH release, but a small increase in FTL release.

These results are very preliminary, and more independent experiments need to be performed. Furthermore, mRNA and intracellular protein evaluation would be important to better help clarify the processes involved.

Nonetheless, the activation of NF-κB by TNF-α might be behind the slightly increased release of FTH in consequence of its upregulation. The FSL-1 effects are in contrast with this notion.

Moreover, we quantified iron intracellular levels in BMM treated with FAC, infected with *M. avium* (Figure 21), and in LSEC stimulated with inflammatory factors (Figure 22).

Treatment with FAC actually led to an increase in iron content in macrophages. The fact that we did not observe appreciable differences in the synthesis and release of FT can either be due to the fact that iron overload is not sufficient to trigger that response or because the treatment was not long enough.

Infection with *M. avium* leads to a modest decrease in intracellular iron content in macrophages. Although the decrease is almost negligible and experiments with a longer infection period need to be performed, this data comprises a small corroboration of the hypothesis in which infected macrophages release their iron to starve the intracellular bacteria.

Interestingly, in LSEC, the preliminary data showed that inflammation seems to result in a slight decrease in intracellular iron content.

Finally, we focused on dissecting the iron intercellular communication between hepatocytes and LSEC or BMM.

For studying hepatocyte–LSEC communication, we used conditioned media experiments (Figure 23A). These kinds of experiments allow us to understand how factors released by LSEC influence iron-related gene expression in the hepatocytes. To obtain conditioned media, cells are cultured in normal conditions or with some type of stimuli. In this case, LSEC were treated with TNF-α or FSL-1.

Notably, as controls, we incubated hepatocytes with complete William's E and with complete William's E with VEGF. This second control is crucial to rule out any interference of the growth factor VEGF, present in LSEC conditioned media. Importantly, the presence of VEGF in LSEC media is indispensable once LSEC, in the absence of the growth factor, start to trans differentiate, which could affect the results. The trans differentiation, besides leading to the loss of LSEC-specific markers, leads to a shift from an anti-inflammatory to a pro-inflammatory phenotype in LSEC [111]. Thus, if LSEC are transdifferentiated, we would not be able to understand if the results are due to the inflammatory stimuli or to the changes inherent to the trans differentiation.

The effects of LSEC conditioned media on hepatocyte gene expression were not very marked and had some variability, which is inevitable when working with primary cell lines. Additional experiments should be performed in order to confirm the observed trends.

The most noteworthy alterations occurred in the expression of *Fth1* and *Fpn* genes. The incubation of hepatocytes with the conditioned medium from non-treated LSEC tended to increase the expression of both genes. However, this induction was lower in the case of conditioned media obtained from LSEC treated with inflammatory stimuli. *Ftl* and *Bmp6* expression in hepatocytes was not significantly altered by incubation with LSEC conditioned medium. However, they tended to decrease when hepatocytes were exposed to supernatants from LSEC treated with FSL-1. Of note, VEGF alone tended to induce an overall decrease in gene expression in hepatocytes, which should be further

investigated in future studies. The exception is *Tfr1,* whose expression remained unchanged with all the treatments.

LSEC are capable of releasing pro-inflammatory factors, so we expect that upon inflammatory stimuli, their conditioned media will contain those factors. In consequence, those factors would impact iron-related gene expression in the hepatocytes they come into contact with. Thus, we would expect a similar pattern to the one observed in hepatocytes under inflammation in response to other factors. This is not the case for *Fth1* expression; therefore we hypothesize that LSEC are releasing factor(s) that lead to *Fth1* downregulation. Moreover, *Fpn* upregulation upon LSEC conditioned treatments suggests some factor produced by the endothelial cells has a greater impact on hepatocytes than the pro-inflammatory factors.

To study the communication between hepatocytes and macrophages, we used a co-culture system with trans well inserts (Figure 23B). As previously discussed, in this system, both cell types share the same media and are impacted by each other.

An important challenge that we faced has to do with the fact that macrophages and primary hepatocytes usually require different media. For BMM, we use DMEM, and for hepatocytes, we use William´s E.

Due to this fact, together with the lack of statistically significant differences between gene expression in hepatocytes when cultured with non-infected and infected BMM, could lead us to believe that the small differences observed have to do with the media question. It would be important to further optimize the co-culture and find a media suitable for both cell types.

Nonetheless, hepatocytes seemed to under express *Fth1*, maintain *Ftl* expression, and upregulate *Tfr1* when co-cultured with infected macrophages. *Bmp6* and *Fpn* showed high variability between independent experiments, and more experiments should be performed.

These results are somewhat concordant with the ones obtained by LPS treatment. So, *Tfr1* upregulation is probably due to the effects of inflammatory factors released by BMM in the hepatocytes.

Conclusion and Future Perspectives

In a retrospective analysis, the initial aims of this project were too ambitious and several technical drawbacks unabled their full achievement.

The project allowed me to learn a wide variety of techniques, from primary cell isolation and culture, to real-time PCR, through western blot, ELISA, and flow cytometry, among others.

Moreover, the preliminary results obtained indicate that this is a relevant topic, worth a deeper investigation. They will guide the design of the much-needed future studies to be performed.

In these future studies, it will be important to:

1. Perform additional experiments with each of the cell types alone, for the optimization of the stimuli and timings most suitable for the analysis of iron-related alterations.
2. In the same assays, perform a more systematic analysis of gene expression, intracellular protein, extracellular protein, and iron levels, in the same conditions, to have a full picture of the alterations induced by each stimulus.
3. Optimize the differential quantification of FTH and FTL proteins, clarifying eventual artifacts inherent to the currently available method.
4. After these experiments on individual cell types, proceed with the exposure of each cell type to the supernatants from other cells. For this, it is crucial to previously identify a medium that can be used in all cultures, independently of cell type.
5. Finally, co-cultures between the different cell types should be established.
6. Moreover, it would be interesting to consider the hypothesis of a spheroid with different liver cell populations.

References

1. Fonseca, Ó., et al., *New Perspectives on Circulating Ferritin: Its Role in Health and Disease.* Molecules, 2023. **28**(23).
2. Teh, M.R., A.E. Armitage, and H. Drakesmith, *Why cells need iron: a compendium of iron utilisation.* Trends Endocrinol Metab, 2024. **35**(12): p. 1026-1049.
3. Hentze, M.W., M.U. Muckenthaler, and N.C. Andrews, *Balancing acts: molecular control of mammalian iron metabolism.* Cell, 2004. **117**(3): p. 285-97.
4. Muckenthaler, M.U., et al., *A Red Carpet for Iron Metabolism.* Cell, 2017. **168**(3): p. 344-361.
5. Kawabata, H., *Transferrin and transferrin receptors update.* Free Radic Biol Med, 2019. **133**: p. 46-54.
6. Worthen, C.A. and C.A. Enns, *The role of hepatic transferrin receptor 2 in the regulation of iron homeostasis in the body.* Front Pharmacol, 2014. **5**: p. 34.
7. Vogt, A.S., et al., *On Iron Metabolism and Its Regulation.* Int J Mol Sci, 2021. **22**(9).
8. Corna, G., et al., *Polarization dictates iron handling by inflammatory and alternatively activated macrophages.* Haematologica, 2010. **95**(11): p. 1814-22.
9. Bou-Abdallah, F., *The iron redox and hydrolysis chemistry of the ferritins.* Biochim Biophys Acta, 2010. **1800**(8): p. 719-31.
10. Wang, W., et al., *Serum ferritin: Past, present and future.* Biochim Biophys Acta, 2010. **1800**(8): p. 760-9.
11. Wang, D., et al., *Caspse-11-GSDMD pathway is required for serum ferritin secretion in sepsis.* Clin Immunol, 2019. **205**: p. 148-152.
12. Yanatori, I., et al., *CD63 is regulated by iron via the IRE-IRP system and is important for ferritin secretion by extracellular vesicles.* Blood, 2021. **138**(16): p. 1490-1503.
13. Mukherjee, C., et al., *Oligodendrocytes Provide Antioxidant Defense Function for Neurons by Secreting Ferritin Heavy Chain.* Cell Metab, 2020. **32**(2): p. 259-272.e10.
14. Palsa, K., et al., *H-ferritin in sows' colostrum- and milk-derived extracellular vesicles: a novel iron delivery concept.* J Anim Sci, 2023. **101**.
15. Gurung, S., et al., *The exosome journey: from biogenesis to uptake and intracellular signalling.* Cell Commun Signal, 2021. **19**(1): p. 47.
16. Hagen, W.R., *Maximum iron loading of ferritin: half a century of sustained citation distortion.* Metallomics, 2022. **14**(9).
17. Levi, S., et al., *Mechanism of ferritin iron uptake: activity of the H-chain and deletion mapping of the ferro-oxidase site. A study of iron uptake and ferro-oxidase activity of human liver, recombinant H-chain ferritins, and of two H-chain deletion mutants.* J Biol Chem, 1988. **263**(34): p. 18086-92.
18. Mehlenbacher, M., et al., *Iron Oxidation and Core Formation in Recombinant Heteropolymeric Human Ferritins.* Biochemistry, 2017. **56**(30): p. 3900-3912.
19. Mancias, J.D., et al., *Quantitative proteomics identifies NCOA4 as the cargo receptor mediating ferritinophagy.* Nature, 2014. **509**(7498): p. 105-9.
20. Gomes, A.C., et al., *Modulation of Iron Metabolism in Response to Infection: Twists for All Tastes.* Pharmaceuticals (Basel), 2018. **11**(3).
21. Brasse-Lagnel, C., et al., *Intestinal DMT1 cotransporter is down-regulated by hepcidin via proteasome internalization and degradation.* Gastroenterology, 2011. **140**(4): p. 1261-1271.e1.
22. Steinbicker, A.U. and M.U. Muckenthaler, *Out of balance--systemic iron homeostasis in iron-related disorders.* Nutrients, 2013. **5**(8): p. 3034-61.

23. Xiao, X., V.M. Alfaro-Magallanes, and J.L. Babitt, *Bone morphogenic proteins in iron homeostasis.* Bone, 2020. **138**: p. 115495.
24. Babitt, J.L., et al., *Bone morphogenetic protein signaling by hemojuvelin regulates hepcidin expression.* Nat Genet, 2006. **38**(5): p. 531-9.
25. Nemeth, E., et al., *IL-6 mediates hypoferremia of inflammation by inducing the synthesis of the iron regulatory hormone hepcidin.* J Clin Invest, 2004. **113**(9): p. 1271-6.
26. Verga Falzacappa, M.V., et al., *STAT3 mediates hepatic hepcidin expression and its inflammatory stimulation.* Blood, 2007. **109**(1): p. 353-8.
27. Lee, Y.S., et al., *Hepatocyte toll-like receptor 4 mediates lipopolysaccharide-induced hepcidin expression.* Exp Mol Med, 2017. **49**(12): p. e408.
28. Moreira, A.C., et al., *Hepcidin-(In)dependent Mechanisms of Iron Metabolism Regulation during Infection by Listeria and Salmonella.* Infect Immun, 2017. **85**(9).
29. Peyssonnaux, C., et al., *TLR4-dependent hepcidin expression by myeloid cells in response to bacterial pathogens.* Blood, 2006. **107**(9): p. 3727-32.
30. Michels, K.R., et al., *Hepcidin-mediated iron sequestration protects against bacterial dissemination during pneumonia.* JCI Insight, 2017. **2**(6): p. e92002.
31. Armitage, A.E., et al., *Hepcidin regulation by innate immune and infectious stimuli.* Blood, 2011. **118**(15): p. 4129-39.
32. Ganz, T., *Erythropoietic regulators of iron metabolism.* Free Radic Biol Med, 2019. **133**: p. 69-74.
33. Srole, D.N. and T. Ganz, *Erythroferrone structure, function, and physiology: Iron homeostasis and beyond.* J Cell Physiol, 2021. **236**(7): p. 4888-4901.
34. Wang, C.Y., et al., *Erythroferrone lowers hepcidin by sequestering BMP2/6 heterodimer from binding to the BMP type I receptor ALK3.* Blood, 2020. **135**(6): p. 453-456.
35. Liu, Q., et al., *Hypoxia-inducible factor regulates hepcidin via erythropoietin-induced erythropoiesis.* J Clin Invest, 2012. **122**(12): p. 4635-44.
36. Chiabrando, D., et al., *Cell-specific regulation of Ferroportin transcription following experimentally-induced acute anemia in mice.* Blood Cells Mol Dis, 2013. **50**(1): p. 25-30.
37. Shah, Y.M. and L. Xie, *Hypoxia-inducible factors link iron homeostasis and erythropoiesis.* Gastroenterology, 2014. **146**(3): p. 630-42.
38. Li, X., et al., *NCOA4 is regulated by HIF and mediates mobilization of murine hepatic iron stores after blood loss.* Blood, 2020. **136**(23): p. 2691-2702.
39. Das, N.K., et al., *Modulation of the HIF2α-NCOA4 axis in enterocytes attenuates iron loading in a mouse model of hemochromatosis.* Blood, 2022. **139**(16): p. 2547-2552.
40. Kruepunga, N., et al., *Anatomy of rodent and human livers: What are the differences?* Biochim Biophys Acta Mol Basis Dis, 2019. **1865**(5): p. 869-878.
41. Martini, T., F. Naef, and J.S. Tchorz, *Spatiotemporal Metabolic Liver Zonation and Consequences on Pathophysiology.* Annu Rev Pathol, 2023. **18**: p. 439-466.
42. Gong, J., et al., *Hepatocytes: A key role in liver inflammation.* Front Immunol, 2022. **13**: p. 1083780.
43. Jetter, A. and G.A. Kullak-Ublick, *Drugs and hepatic transporters: A review.* Pharmacol Res, 2020. **154**: p. 104234.
44. Shulpekova, Y., et al., *A Recent Ten-Year Perspective: Bile Acid Metabolism and Signaling.* Molecules, 2022. **27**(6): p. 1983.
45. Zhou, Z., M.J. Xu, and B. Gao, *Hepatocytes: a key cell type for innate immunity.* Cell Mol Immunol, 2016. **13**(3): p. 301-15.
46. Jiang, M., et al., *Hepatocyte reprogramming in liver regeneration: Biological mechanisms and applications.* Febs j, 2023. **290**(24): p. 5674-5688.

47. Gissen, P. and I.M. Arias, *Structural and functional hepatocyte polarity and liver disease.* J Hepatol, 2015. **63**(4): p. 1023-37.
48. Su, T., et al., *Single-Cell Transcriptomics Reveals Zone-Specific Alterations of Liver Sinusoidal Endothelial Cells in Cirrhosis.* Cell Mol Gastroenterol Hepatol, 2021. **11**(4): p. 1139-1161.
49. He, Q., et al., *Role of liver sinusoidal endothelial cell in metabolic dysfunction-associated fatty liver disease.* Cell Commun Signal, 2024. **22**(1): p. 346.
50. Szafranska, K., et al., *The wHole Story About Fenestrations in LSEC.* Front Physiol, 2021. **12**: p. 735573.
51. Poisson, J., et al., *Liver sinusoidal endothelial cells: Physiology and role in liver diseases.* J Hepatol, 2017. **66**(1): p. 212-227.
52. McConnell, M.J., et al., *The evolving role of liver sinusoidal endothelial cells in liver health and disease.* Hepatology, 2023. **78**(2): p. 649-669.
53. Colucci, S., et al., *Iron-dependent BMP6 Regulation in Liver Sinusoidal Endothelial Cells Is Instructed by Hepatocyte-derived Secretory Signals.* Hemasphere, 2022. **6**(10): p. e773.
54. Colucci, S., et al., *Liver Sinusoidal Endothelial Cells Suppress Bone Morphogenetic Protein 2 Production in Response to TGFβ Pathway Activation.* Hepatology, 2021. **74**(4): p. 2186-2200.
55. Krenkel, O. and F. Tacke, *Liver macrophages in tissue homeostasis and disease.* Nat Rev Immunol, 2017. **17**(5): p. 306-321.
56. Dixon, L.J., et al., *Kupffer cells in the liver.* Compr Physiol, 2013. **3**(2): p. 785-97.
57. Lan, T., et al., *Role of Immune Cells in Biliary Repair.* Front Immunol, 2022. **13**: p. 866040.
58. Kamm, D.R. and K.S. McCommis, *Hepatic stellate cells in physiology and pathology.* J Physiol, 2022. **600**(8): p. 1825-1837.
59. Zhang, Y., et al., *Signaling pathways that activate hepatic stellate cells during liver fibrosis.* Front Med (Lausanne), 2024. **11**: p. 1454980.
60. Silva, I., et al., *IL-1 beta-mediated macrophage-hepatocyte crosstalk upregulates hepcidin under physiological low oxygen levels.* Redox Biol, 2019. **24**: p. 101209.
61. Ghosh, P., et al., *Inflammatory macrophage to hepatocyte signals can be prevented by extracellular vesicle reprogramming.* J Cell Sci, 2023. **136**(9).
62. Tarasenko, T.N., et al., *Macrophage derived TNFα promotes hepatic reprogramming to Warburg-like metabolism.* J Mol Med (Berl), 2019. **97**(9): p. 1231-1243.
63. Rex, J., et al., *IL-1β and TNFα Differentially Influence NF-κB Activity and FasL-Induced Apoptosis in Primary Murine Hepatocytes During LPS-Induced Inflammation.* Front Physiol, 2019. **10**: p. 117.
64. Chen, S., et al., *Macrophages in immunoregulation and therapeutics.* Signal Transduct Target Ther, 2023. **8**(1): p. 207.
65. Gidon, A., et al., *The Tumor Necrosis Factor Alpha and Interleukin 6 Auto-paracrine Signaling Loop Controls Mycobacterium avium Infection via Induction of IRF1/IRG1 in Human Primary Macrophages.* mBio, 2021. **12**(5): p. e0212121.
66. Li, X., H. Körner, and X. Liu, *Susceptibility to Intracellular Infections: Contributions of TNF to Immune Defense.* Front Microbiol, 2020. **11**: p. 1643.
67. Ehlting, C., S.D. Wolf, and J.G. Bode, *Acute-phase protein synthesis: a key feature of innate immune functions of the liver.* Biol Chem, 2021. **402**(9): p. 1129-1145.
68. Shen, X., et al., *Iron metabolism and ferroptosis in nonalcoholic fatty liver disease: what is our next step?* Am J Physiol Endocrinol Metab, 2024. **326**(6): p. E767-e775.
69. Sun, K., et al., *Iron homeostasis in arthropathies: From pathogenesis to therapeutic potential.* Ageing Res Rev, 2021. **72**: p. 101481.

70. Portolés, J., et al., *Anemia in Chronic Kidney Disease: From Pathophysiology and Current Treatments, to Future Agents.* Front Med (Lausanne), 2021. **8**: p. 642296.
71. Wynn, T.A., A. Chawla, and J.W. Pollard, *Macrophage biology in development, homeostasis and disease.* Nature, 2013. **496**(7446): p. 445-55.
72. Ludwig, N., et al., *Iron scavenging and myeloid cell polarization.* Trends Immunol, 2024. **45**(8): p. 625-638.
73. Kramer, J., Ö. Özkaya, and R. Kümmerli, *Bacterial siderophores in community and host interactions.* Nat Rev Microbiol, 2020. **18**(3): p. 152-163.
74. Guida, C., et al., *A novel inflammatory pathway mediating rapid hepcidin-independent hypoferremia.* Blood, 2015. **125**(14): p. 2265-75.
75. Harrington-Kandt, R., et al., *Hepcidin deficiency and iron deficiency do not alter tuberculosis susceptibility in a murine M.tb infection model.* PLoS One, 2018. **13**(1): p. e0191038.
76. Rodrigues, P.N., et al., *Mycobacteria-induced anaemia revisited: a molecular approach reveals the involvement of NRAMP1 and lipocalin-2, but not of hepcidin.* Immunobiology, 2011. **216**(10): p. 1127-34.
77. Chlosta, S., et al., *The iron efflux protein ferroportin regulates the intracellular growth of Salmonella enterica.* Infect Immun, 2006. **74**(5): p. 3065-7.
78. Murdoch, C.C. and E.P. Skaar, *Nutritional immunity: the battle for nutrient metals at the host-pathogen interface.* Nat Rev Microbiol, 2022. **20**(11): p. 657-670.
79. Flo, T.H., et al., *Lipocalin 2 mediates an innate immune response to bacterial infection by sequestrating iron.* Nature, 2004. **432**(7019): p. 917-21.
80. Meng, C., et al., *The expression of Nramp1 modulates the uptake of Mycobacterium tuberculosis by macrophages through alternating inflammatory responses.* Tuberculosis (Edinb), 2023. **143**: p. 102414.
81. To, K., et al., *General Overview of Nontuberculous Mycobacteria Opportunistic Pathogens: Mycobacterium avium and Mycobacterium abscessus.* J Clin Med, 2020. **9**(8).
82. Neyrolles, O., et al., *Mycobacteria, metals, and the macrophage.* Immunol Rev, 2015. **264**(1): p. 249-63.
83. Busatto, C., et al., *Mycobacterium avium: an overview.* Tuberculosis (Edinb), 2019. **114**: p. 127-134.
84. Appelberg, R., *Macrophage nutriprive antimicrobial mechanisms.* J Leukoc Biol, 2006. **79**(6): p. 1117-28.
85. Flórido, M. and R. Appelberg, *Granuloma necrosis during Mycobacterium avium infection does not require tumor necrosis factor.* Infect Immun, 2004. **72**(10): p. 6139-41.
86. Cronan, M.R., et al., *Macrophage Epithelial Reprogramming Underlies Mycobacterial Granuloma Formation and Promotes Infection.* Immunity, 2016. **45**(4): p. 861-876.
87. Egen, J.G., et al., *Macrophage and T cell dynamics during the development and disintegration of mycobacterial granulomas.* Immunity, 2008. **28**(2): p. 271-84.
88. Gomes-Pereira, S., et al., *Increased susceptibility to Mycobacterium avium in hemochromatosis protein HFE-deficient mice.* Infect Immun, 2008. **76**(10): p. 4713-9.
89. Mesquita, G., et al., *H-Ferritin is essential for macrophages' capacity to store or detoxify exogenously added iron.* Sci Rep, 2020. **10**(1): p. 3061.
90. Silva-Gomes, S., et al., *Mycobacterium avium infection induces H-ferritin expression in mouse primary macrophages by activating Toll-like receptor 2.* PLoS One, 2013. **8**(12): p. e82874.
91. Moreira, A.C., et al., *H-Ferritin Produced by Myeloid Cells Is Released to the Circulation and Plays a Major Role in Liver Iron Distribution during Infection.* Int J Mol Sci, 2021. **23**(1).

92. Harper, J.M., *Primary Cell Culture as a Model System for Evolutionary Molecular Physiology.* Int J Mol Sci, 2024. **25**(14).
93. Piwocka, O., et al., *Navigating challenges: optimising methods for primary cell culture isolation.* Cancer Cell Int, 2024. **24**(1): p. 28.
94. Verma, A., M. Verma, and A. Singh, *Animal tissue culture principles and applications Animal Biotechnology Tools and Techniques*. 2020, Academic Press: Cambridge, MA. p. 269-293.
95. Bekedam, F.T., et al., *Mechanical stimulation of induced pluripotent stem derived cardiac fibroblasts.* Sci Rep, 2024. **14**(1): p. 9795.
96. Ding, T., et al., *Comprehensive review of macrophage models: primary cells and immortalized lines across species.* Front Immunol, 2025. **16**: p. 1640935.
97. Charni-Natan, M. and I. Goldstein, *Protocol for Primary Mouse Hepatocyte Isolation.* STAR Protoc, 2020. **1**(2): p. 100086.
98. Richter, M., et al., *From Donor to the Lab: A Fascinating Journey of Primary Cell Lines.* Front Cell Dev Biol, 2021. **9**: p. 711381.
99. Corrò, C., L. Novellasdemunt, and V.S.W. Li, *A brief history of organoids.* Am J Physiol Cell Physiol, 2020. **319**(1): p. C151-c165.
100. Ma, C., et al., *Organ-on-a-Chip: A New Paradigm for Drug Development.* Trends Pharmacol Sci, 2021. **42**(2): p. 119-133.
101. Cheng, C.K., et al., *Biophysical and Biochemical Roles of Shear Stress on Endothelium: A Revisit and New Insights.* Circ Res, 2025. **136**(7): p. 752-772.
102. Guo, Q., et al., *Isolation and Characterization of Mouse Primary Liver Sinusoidal Endothelial Cells.* J Vis Exp, 2021(178).
103. Charlebois, E., et al., *Liver sinusoidal endothelial cells induce BMP6 expression in response to non-transferrin-bound iron.* Blood, 2023. **141**(3): p. 271-284.
104. Liu, Y., et al., *Excess iron intake induced liver injury: The role of gut-liver axis and therapeutic potential.* Biomed Pharmacother, 2023. **168**: p. 115728.
105. Recalcati, S. and G. Cairo, *Macrophages and Iron: A Special Relationship.* Biomedicines, 2021. **9**(11).
106. Cohen, L.A., et al., *Serum ferritin is derived primarily from macrophages through a nonclassical secretory pathway.* Blood, 2010. **116**(9): p. 1574-84.
107. Moreira, A.C., G. Mesquita, and M.S. Gomes, *Ferritin: An Inflammatory Player Keeping Iron at the Core of Pathogen-Host Interactions.* Microorganisms, 2020. **8**(4).
108. Bonitz, K., et al., *Hepatocyte Toll-like receptors contribute to the hepcidin inflammatory response to pathogens and pathogen-derived ligands.* Hemasphere, 2025. **9**(4): p. e70096.
109. Liao, Y., et al., *Ferritin's role in infectious diseases: Exploring pathogenic mechanisms and clinical implications.* New Microbes New Infect, 2025. **65**: p. 101582.
110. Drakesmith, H., E. Nemeth, and T. Ganz, *Ironing out Ferroportin.* Cell Metab, 2015. **22**(5): p. 777-87.
111. Wilkinson, A.L., M. Qurashi, and S. Shetty, *The Role of Sinusoidal Endothelial Cells in the Axis of Inflammation and Cancer Within the Liver.* Front Physiol, 2020. **11**: p. 990.